AGU PUBLICATIONS

Geochemistry, Geophysics, Geosystems

RESEARCH ARTICLE
10.1002/2015GC005828

Constraints on the evolution of crustal flow beneath Northern Tibet

Florian Le Pape[1], Alan G. Jones[1,2], Martyn J. Unsworth[3], Jan Vozar[1], Wenbo Wei[4], Sheng Jin[4], Gaofeng Ye[4], Jianen Jing[4], Hao Dong[4], Letian Zhang[4], and Chengliang Xie[4]

[1]Dublin Institute for Advanced Studies, School of Cosmic Physics, Geophysics Section, Dublin, Ireland, [2]Now at Complete MT Solutions, [3]Department of Physics, University of Alberta, Edmonton, Alberta, Canada, [4]School of Geophysics and Information Technology, China University of Geosciences, Beijing, China

Key Points:
- Magnetotelluric models in northern Tibet are combined with laboratory studies
- Constraints on melt fraction, temperature, and crustal flow patterns are proposed
- Discussion on proportion of crustal flow injected beneath the Kunlun fault

Correspondence to:
F. Le Pape,
flepape@cp.dias.ie

Citation:
Le Pape, F., A. G. Jones, M. J. Unsworth, J. Vozar, W. Wei, J. Sheng, G. Ye, J. Jing, H. Dong, L. Zhang, and C. Xie (2015), Constraints on the evolution of crustal flow beneath Northern Tibet, *Geochem. Geophys. Geosyst.*, *16*, doi:10.1002/2015GC005828.

Received 3 APR 2015
Accepted 2 NOV 2015
Accepted article online 5 NOV 2015

© 2015. American Geophysical Union. All Rights Reserved.

Abstract Crustal flow is an important tectonic process active in continent-continent collisions and which may be significant in the development of convergent plate boundaries. In this study, the results from multi-dimensional electrical conductivity modeling have been combined with laboratory studies of the rheology of partially molten rocks to characterize the rheological behavior of the middle-to-lower crust of both the Songpan-Ganzi and Kunlun terranes in the northern Tibetan Plateau. Two different methods are adopted to develop constraints on melt fraction, temperature, and crustal flow velocity in the study area. The estimates of these parameters are then used to evaluate whether crustal flow can occur on the northern margin of the Tibetan plateau. In the Songpan-Ganzi crust, all conditions are satisfied for topography-driven channel flow to be dominant, with partial melt not being required for flow at temperature above 1000°C. Further north, the Kunlun fault defines the southern boundary of a transition zone between the Tibetan plateau and the Qaidam basin. Constrained by the estimated melt fractions, it is shown that channel injection across the fault requires temperatures close to 900°C. The composition of igneous rocks found at the surface confirm those conditions are met for the southern Kunlun ranges. To the north, the Qaidam basin is characterized by colder crust that may reflect an earlier stage in the channel injection process. In the study area, at least 10% of the eastward directed Tibetan crustal flow could be deflected northward across the Kunlun Fault and injected into the transition zone defining the northern margin of the Tibetan plateau.

1. Introduction

One of the keys to interpreting the past and future evolution of continent-continent collisions such as the Tibetan plateau is a complete understanding of the dynamics of their margins. In the case of the Tibetan plateau, fundamental questions remain concerning the geodynamic processes that have controlled its northward growth, and the possible absorption of the Qaidam basin into the flat, highly elevated plateau that currently extends north from the Himalayas to the Kunlun Shan. In a review on the growth of the Tibetan plateau, *Wang et al*. [2014] proposed that the plateau continues to expand, and may have grown southward and northward from a 40 Ma year old proto-plateau formed from the coalesced Lhasa and Qiangtang terranes. *Wang et al*. [2014] also suggest that as long as the collision with India progresses, crustal flow will continue to move crustal material across the tectonic boundaries of the plateau that are characterized by high mountain belts and fault systems bounding the homogeneously highly elevated plateau.

1.1. Crustal Flow in Southern and Eastern Tibet

Following the paradigm-shift created by the detection of partial melt in the middle crust of southern Tibet by *Nelson et al*. [1996], *Beaumont et al*. [2001] proposed that partially molten crust of southern Tibet is being extruded southward to the Himalayas through channel flow, where it is exhumed at the surface. While many researchers support this hypothesis [*Searle et al*., 2011], a number of researchers remain skeptical. For example, *Harrison* [2006] subsequently claimed that there is no significant evidence that supports such model. Also, based on seismic imaging of the Himalayas and southern Tibet, *Nabelek et al*. [2009] interpreted the ductile zones as being too thin to allow crustal flow.

In order to explain the deformation of the eastern Tibetan plateau, *Clark and Royden* [2000] proposed a simple crustal flow model for eastern Tibet, with a weak uniform layer in the Tibetan middle-to-lower crust,

allowing rapid ductile flow in the crust in response to lateral pressure gradients [*Bird*, 1991; *Royden et al*., 1997]. Note that this is different from the previously described flow in the Himalaya, since it is not exhumed and exposed at the surface. The topography-driven channel flow model inferred by *Clark and Royden* [2000] can explain both the topographically steep and shallow margins of the Tibetan plateau. Steep topography occurs in response to blocking of the crustal flow where it meets with the surrounding rigid blocks, such as Tarim to the northwest, Qaidam to the north, and Sichuan to the east. In contrast, the gentle topography of southeast Tibet can be explained by unimpeded flow, escaping to the east, moving around the eastern Himalayan syntaxis and into southeast Tibet [*Royden et al*., 1997; *Clark and Royden*, 2000]. However, magnetotelluric studies in southeast Tibet by *Bai et al*. [2010] have produced conductivity models that suggest that crustal flow in this region of Tibet is spatially more complex than in the model proposed by *Clark and Royden* [2000].

1.2. Crustal Flow in Northern Tibet

Recent geophysical studies in northern Tibet have investigated the Kunlun Fault and raised questions about the structure and evolution of the northern margin of the Tibetan plateau. Using active seismic profiles in northeastern Tibet (102°E–104°E), *Wang et al*. [2011] and *Gao et al*. [2013] imaged the presence of dipping reflectors in the middle and lower crust. As a consequence, the authors interpreted those observations as being inconsistent with the occurrence of channel flow and suggested that such processes are not necessary to explain the current elevation of the area. However, further west, both seismic and magnetotelluric INDEPTH-IV studies have revealed the presence of horizontal low-velocity/high-conductivity zones interpreted as partially molten crust extending across the Kunlun fault system. From INDEPTH IV wide-angle seismic data, *Karplus et al*. [2011] inferred injection of Songpan-Ganzi crust beneath the Kunlun Shan as far as a Moho step located beneath the southern boundary of the Qaidam basin (36.6°N). Based on ambient noise seismic tomography results, *Jiang et al*. [2014] defined a low-velocity zone (LVZ) that extended north across the surface trace of the Kunlun fault between 92°E and 104°E. Furthermore, the observed LVZ is characterized by significant east-west variations along-strike and parallel to the fault. These results are in good agreement with the conductivity models of *Le Pape et al*. [2012] and *Wei et al*. [2014], derived from INDEPTH-III and INDEPTH-IV MT data, that revealed heterogeneous distribution of a midlower crustal conductive anomaly beneath the Kunlun fault, and that was interpreted as the northward penetration of the partially molten Tibetan crust. Petrological support for presence of felsic partial melt in the crust beneath the Kunlun Fault comes from *Wang et al*. [2012] who reported the presence of rhyolitic igneous rocks as young as 1.5 Ma in the vicinity of the Kunlun system.

Those observations are particularly interesting because they can be directly related to the channel injection model of *Medvedev and Beaumont* [2006] to explain the evolution of the transition zone between the Northern Tibetan plateau and the foreland defined by the Qaidam basin. One of the main questions raised by *Medvedev and Beaumont* [2006] was whether the pressure gradient associated with the steep topography of the margins of the plateau was high enough to cause northward channel injection of the Tibetan Crust, despite the higher effective viscosity of the Kunlun Block. Although *Medvedev and Beaumont* [2006] successfully managed to numerically model the thickening and widening of the plateau as the transition zone migrated north due to channel injection, it remains uncertain if such a process is actually occurring on the northern margin of the Tibetan Plateau.

1.3. Geophysical Constraints on Rheology

To address the question of crustal flow in northern Tibet, geophysical data that can constrain rheology are required. Magnetotellurics (MT) is one such method, since measurements of electrical conductivity can be linked to rheology due to their joint Arrhenius exponential dependence on temperature, as first proposed by *Tozer* [1979, 1981]. *Unsworth et al*. [2005] used estimates of melt fraction in Southern Tibet to derive constraints on crustal strength and effective viscosity. This approach was expanded upon and described in more detail in *Rippe and Unsworth* [2010], where the authors established a direct relationship between conductance and flow velocity in order to quantify crustal flow in Tibet.

Although electrical conductivity and viscosity of a rock are both dependent on temperature and on melt content composition, there are few studies that have effectively linked magnetotelluric interpretation to geodynamics. *Pommier et al*. [2013] proposed a model to relate electrical conductivity with viscosity as a function of temperature and composition, including water content. The model was mainly developed for systems with

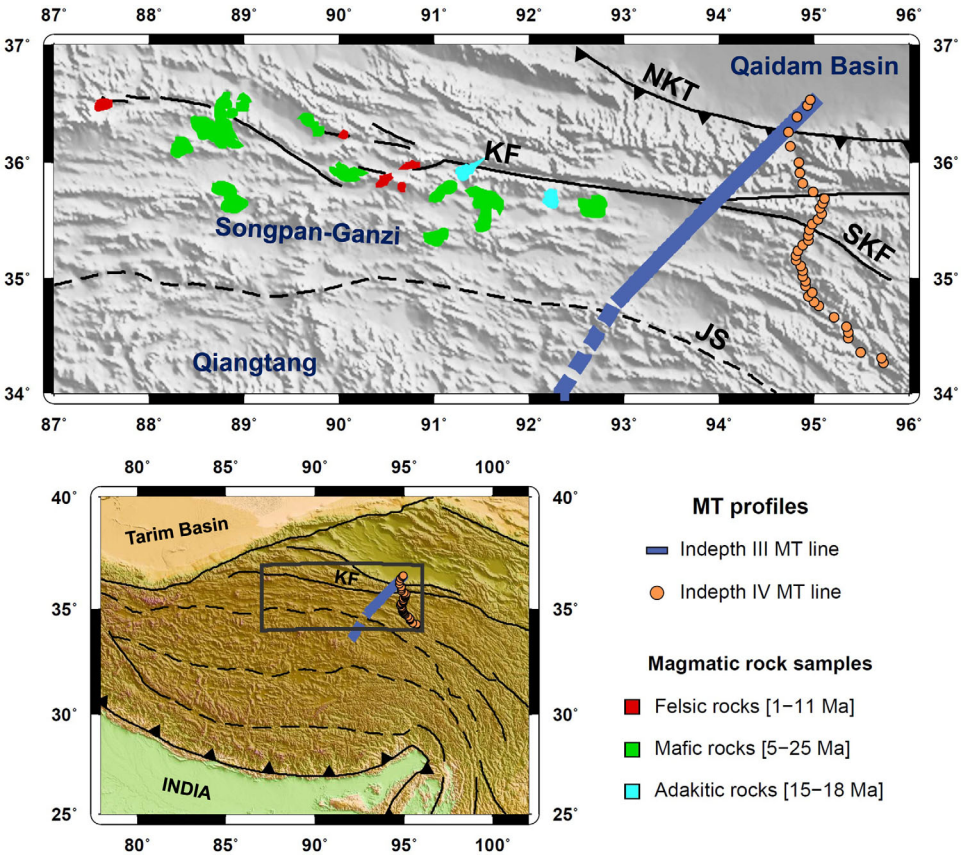

Figure 1. Topographic map of the study area showing the location of the INDEPTH MT profiles [*Le Pape et al.*, 2012; *Wei et al.*, 2014] as well as the exposures of different types of igneous rocks: mafic rocks [*Guo et al.*, 2006], adakitic rocks [*Wang et al.*, 2005], and felsic rocks [*Wang et al.*, 2012]. The areas covered by the magmatic rocks on the map have been slightly increased for better reading of their location. JS = Jinsha Suture, SKF = South Kunlun Fault, KF= Kunlun Fault, and NKT = North Kunlun Fault.

melt fractions above 0.7 (i.e., 70% molten) where the bulk conductivity and viscosity are directly controlled by both melt conductivity and melt viscosity, respectively. Despite limitations in differentiating melt compositions directly from the MT data, *Pommier et al.* [2013] showed that relating known compositions with conductivities derived from MT can provide useful constraints on the rheological behavior of magma bodies. For Tibet and the particular area of interest, melt fractions in the crust are definitely lower [*Unsworth et al.*, 2005; *Wei et al.*, 2014] and therefore the *Pommier et al.* [2013] relation cannot be directly applied to the study area. However, even for lower melt fractions, composition effects on melt conductivity will still have a significant impact on the bulk conductivity of a two-phase media [*Pommier and Trong*, 2011].

1.4. Objective

The main objective of this paper is to develop improved constraints on the possible occurrence and geometry of channel flow at the northern margin of the Tibetan plateau, and to determine if conditions are met to allow crustal material to flow from the Songpan-Ganzi terrane into the Kunlun block, further north of the Kunlun fault. The study begins with a discussion on evidence for the presence of partial melt in the crust of central and northern Tibet, leading to the assumptions made to determine melt electrical conductivity in the area of interest as a function of temperature, pressure, and composition, including water content in the melt. Melt conductivity is then combined with well-constrained multidimensionality conductivity models of northern Tibet developed from the INDEPTH III and IV magnetotelluric data (Figure 1) [*Le Pape et al.*, 2012; *Wei et al.*, 2014] to estimate the range of melt fractions responsible for the observed high-electrical conductivity in the crust of northern Tibet. After defining crustal flow patterns, this study discusses the conditions under which Poiseuille, or topography-driven, flow could be dominant in northern Tibet. Two different approaches are used to determine the behavior of Poiseuille velocity flow for non-Newtonian fluids. Based on several laboratory studies, a similar method to that employed by *Rippe and Unsworth* [2010] is used to

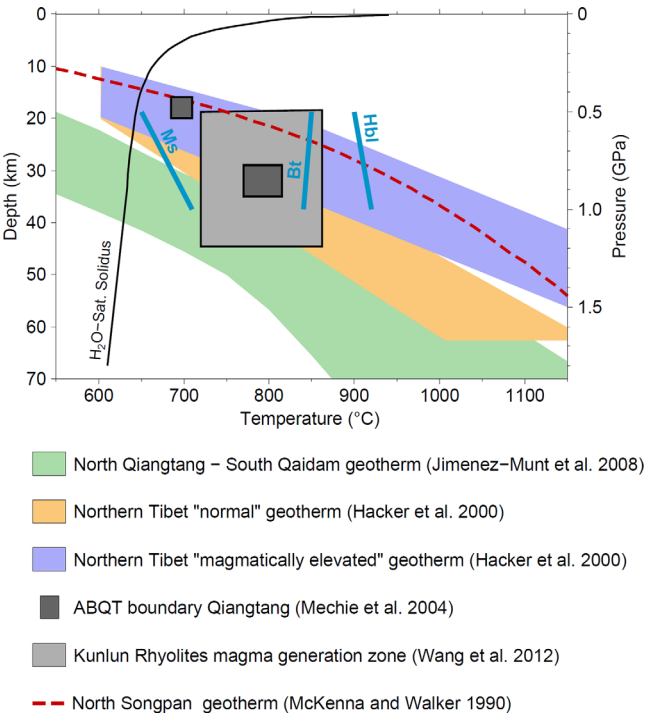

Figure 2. Pressure and temperature characterization of the crust in northern Tibet illustrated by different studies. Dehydration reactions associated with muscovite (Ms), biotite (Bt), and hornblende (Hbl) are derived from *Clemens and Vielzeuf* [1987] for pressure between 500 MPa and 1Ga.

relate Poiseuille flow velocity to melt fraction. The approach of *Rippe and Unsworth* [2010] did not include temperature in the estimates. We extend their work by introducing an empirical flow law based on laboratory measurements [*Rutter et al*., 2006] to calculate flow velocity as a function of temperature and melt fraction. This paper also estimates the proportion of the overall crustal flow that may be crossing the Kunlun fault by comparing effects from melt fraction and temperature differences between both Songpan-Ganzi and Kunlun blocks.

2. Constraints on the Melt Electrical Conductivity in Northern Tibet

2.1. Evidence for the Presence of Crustal Partial Melt in Northern Tibet

Li et al. [2003] showed that metallic minerals and graphite cannot be excluded as an explanation for the anomalously high crustal conductivity observed in Tibet. However, these materials are only likely to be explanations for the elevated conductivity in localized zones along major tectonic boundaries. In contrast, the conductive anomaly observed in central and northern Tibet is spatially widespread in the crust [*Rippe and Unsworth*, 2010; *Le Pape et al*., 2012; *Wei et al*., 2014]. Also, as recently shown graphite films are not stable at temperatures above 700°C [*Yoshino and Noritake*, 2011]. According to *Yardley and Valley* [1997], petrological evidence is against the presence of ubiquitous free fluids at depths greater than a few kilometers. It should be noted that the observation of rapid high volume deep crustal fluxing in the Juneau gold fields of Alaska, by *Goldfarb et al*. [1991] caused Yardley to reflect on his position that fluids cannot be resident for times on the order of tens of millions of years [*Yardley*, 1991]. Even though if assumed that free water is stable at depths greater than 20 km, under the high temperatures characterizing northern Tibet, it would trigger partial melting and dissolve itself in the melt [*Clemens and Vielzeuf*, 1987; *Holtz et al*., 2001]. Although the presence of bright spots in southern Tibet have been interpreted as evidence for widespread aqueous fluids in the crust [*Makovsky and Klemperer*, 1999], there is no comparable observations in central and northern Tibet from active seismic surveys [*Haines et al*., 2003; *Karplus et al*., 2011]. In order to explain the presence of free fluids in the crust overlying partial melt in southern Tibet, *Gaillard et al*. [2004] suggested that the source of the fluids was the crystallization of leucogranitic magmas just below the solidus. With temperatures in central and northern Tibet known to be higher than in southern Tibet [*Hacker et al*., 2000; *Mechie et al*., 2004; *Jimenez-Munt et al*., 2008; *Agius and Lebedev*, 2013; *Vozar et al*., 2014] and the absence of significant bright spots, we assume that most of the observed conductive anomaly can be explained by partial melt alone. Therefore, the remaining candidate for the observed conductive anomaly is the result of either melting of water-saturated rocks or dehydration melting of hydrous minerals [*Patiño Douce and McCarthy*, 1998]. Common crustal rocks require temperatures above 850°C for fluid absent melting [*Patiño Douce and McCarthy*, 1998], however, muscovite-rich metapelitic rocks will melt at lower temperatures [*Clemens and Vielzeuf*, 1987; *Patiño Douce and McCarthy*, 1998]. As seen on Figure 2, several studies are in agreement that such high temperatures are easily reached in the middle crust of central and northern Tibet. Based on integrated geophysical-petrological modeling of lithosphere-asthenosphere boundary in central Tibet using electromagnetic and seismic data, *Vozar et al*. [2014] reported that compared to southern Tibet, central and probably northern Tibet is

Table 1. Estimations of Melt Conductivity (S/m) Using SIGMELTS Calculation for Different Temperature, Pressure, Compositions, and Water Content[a]

Mafic/Intermediate Samples	Composition SiO_2 (wt %)	Composition Na_2O (wt %)	P/T/H_2O Conditions 900°C/10 kbar	P/T/H_2O Conditions 1000°C/10 kbar	P/T/H_2O Conditions 1100°C/10 kbar
Source Rock Resulting H_2O content (wt %) in melt			Intermediate Bt 4.7	Intermediate/Mafic Bt 4.7/Hbl 6.5	Mafic Hbl 6.5
(a) Damaoshan	58.3	3.97	0.4	0.8/2.2	3.5
Kekaohu	58.57	3.58	0.3	0.7/1.9	3.2
Hoh Xil lake	47.2	3.09	0.8	2.1/2.3	4
Xiangyanghu	52.28	3.29	0.4	0.9/2.3	4
Hehuahu	47.29	3.62	0.8	2/2.3	4
Jingyuhu	46.26	3.79	1.1	2.1/2.3	4
Xiongyingtai	53.35	3.15	0.4	0.8/2.1	3.7
(b) Wuxuefeng	61.28	3.99	0.3	0.7/1.9	3
Wuxuefeng	63.8	3.47	0.2	0.5/1.4	2.3
Hongshuihe	66	3.5	0.2	0.5/1.3	2.1
Hongshuihe	65.12	3.72	0.3	0.5/1.4	2.3
Felsic samples	SiO_2 (wt %)	Na_2O (wt %)	800°C/5 kbar	900°C/10 kbar	1000°C/10 kbar
Source rock			Pelitic	Pelitic/Intermediate	Intermediate
Resulting H_2O content (wt %) in melt			Ms 10.7	Ms 12.1/Bt 4.7	Bt 4.7/Hbl 3.7
(c) Bukadaban	73.13	3.21	2	1.4/0.1	0.2/0.1
Southern Malanshan	71.4	3.15	2	1.4/0.03	0.1/0.05
Hundongliang	72.64	4.17	2	1.4/0.3	0.5/0.3

[a]The magma compositions are taken from (a) mafic [*Guo et al.* 2006], (b) adakitic [*Wang et al.* 2005] and (c) felsic [*Wang et al.* 2012] rock samples highlighted in Figure 1. The P-T conditions are derived from Figure 2. The water contents are referred to *Clemens and Vielzeuf* [1987] as a function of the source rock.

characterized by a relatively thin and dry lithosphere that could have limited crustal melting from release of fluids issued from dehydration of the underlying lithosphere. Based on xenolith and seismic data, *Hacker et al.* [2000, 2014] concluded that partial melt in central Qiangtang is a direct product of fluid-absent melting with a relatively low melt fraction (~2%). Furthermore, felsic surface magmatism observed at the vicinity of the Kunlun fault has been interpreted as issued from dehydration melting [*Wang et al.*, 2012]. Thus, in the area of interest, the presence of partial melt is more than likely related to dehydration or fluid-absent melting.

2.2. Melt Electrical Conductivity Inferred From P-T Conditions, Composition, and Water Content

Pressure and temperature (P-T) conditions characteristic of northern Tibet are illustrated in Figure 2 and inferred from geotherms derived from geophysical and petrological studies. In central Tibet, *Mechie et al.* [2004] constrained temperatures in the upper and middle crust using the α-β quartz transition (ABQT) seismic signature (Figure 2, dark gray-shaded boxes). *Jimenez-Munt et al.* [2008] proposed a model for lithospheric temperature beneath the Tibetan plateau based on elevation, gravity, and geoid anomalies (Figure 2, green swath). *Hacker et al.* [2000] revealed the presence of a very hot crust beneath central and northern Tibet based on measurements on metasedimentary and mafic crustal xenoliths (Figure 2, orange and purple swaths). *McKenna and Walker* [1990] proposed another geotherm for northern Tibet related to the formation of the leucogranitic igneous rocks found in the Ulugh Muztagh Area (Figure 2, dashed red line). Finally, *Wang et al.* [2012] reported temperature and pressure intervals for the formation of the peraluminous rhyolites located in the vicinity of the Kunlun fault system (Figure 2, light gray box).

Most of these studies are consistent in showing that crustal temperatures in northern Tibetan are anomalously high. However, Figure 2 shows that the temperature estimates for the middle and lower crust are widely scattered. Thus, deducing robust temperature profiles for the mid-to-lower crust remains problematic and controversial. Moreover, a broad set of samples of igneous rocks (Figure 1 and Table 1) imply a broad range of crustal melt compositions are present beneath northern Tibet. The samples include igneous rocks derived from mafic to intermediates magmas [*Guo et al.*, 2006], adakites [*Wang et al.*, 2005], and more felsic rocks including peraluminous rhyolites [*Wang et al.*, 2012]. In the literature, melt conductivities between 3 and 10 S/m have previously been considered as representative values for melts at mid-to-lower crustal depths [*Partzsch et al.*, 2000; *Rippe and Unsworth*, 2010; *Bai et al.*, 2010]. In addition to pressure and temperature, it is known that the Na_2O and water content has a major effect on melt conductivity [*Gaillard*, 2004]. As a consequence, melt conductivity can be well constrained if information on temperature, pressure,

and composition are appropriately, and correctly, taken into account. Such calculations can be made with compilations of electrical measurements made in the laboratory, such as SIGMELTS [*Pommier and Trong*, 2011]. This allows the user to calculate the electrical conductivity of melt under specified conditions. The resulting melt conductivity estimates derived from SIGMELTS are summarized in Table 1.

Water content is relatively difficult to evaluate for samples from a particular set of temperature and pressure conditions. As discussed above, in this study it is assumed that most melt generated in the crust of northern Tibet is associated with fluid-absent melting resulting from the breakdown of hydrous minerals, such as muscovite (Ms), biotite (Bt), and hornblende (Hbl) [*Clemens and Vielzeuf*, 1987; *Patiño Douce and McCarthy*, 1998]. During melting, these minerals dehydrate and the water released dissolves into the melt. Whereas pelitic rocks appear to be the most fertile, with the breakdown of muscovite at temperatures as low as 665°C (Figure 2, blue line labeled Ms), dehydration reactions linked with biotite and hornblende (Figure 2, blue lines labeled Bt and Hbf, respectively) will occur at higher temperatures (840°C and 900°C, respectively) [*Clemens and Vielzeuf*, 1987]. Figure 2 illustrates the temperature and pressure dependence of the fluid-absent melting reactions characteristic of each of those minerals for pressures between 500 MPa and 1 GPa, as reported in *Clemens and Vielzeuf* [1987]. Water content in melt depends not only on the type of hydrous phase involved in the melting but also on the type of source rocks; pelitic, quartzofeldspathic (felsic), intermediate, and mafic [*Clemens and Vielzeuf*, 1987]. For example, the Kunlun rhyolites have been interpreted as the result of dehydration melting of mica-bearing metasedimentary rocks [*Wang et al*., 2012]. In fact, despite the lack of similar felsic igneous rocks at the surface of the Songpan-Ganzi terrane, those types of pelitic source rocks are also likely to characterize the upper-to-middle Songpan-Ganzi crust, and felsic magmas could be relatively widespread beneath northern Tibet. Adakites observed just south of the Kunlun Fault system have been interpreted as the result of partial melting of amphibole-bearing eclogites [*Wang et al*., 2005].

Furthermore, mafic to intermediate rocks mapped in the Songpan-Ganzi terrane and the Kunlun terrane have been described as the result of melting of a metasomatically enriched lithospheric mantle source [*Turner et al*., 1996; *Guo et al*., 2006]. Those magmas may not be directly linked to melting within the crust, but due to the complexity of the accretion history of the Tibetan Plateau, linked to earlier episodes of subduction, it is important to consider a range of different melt compositions for estimates of melt conductivities in the crust. The parameters used for the melt conductivity calculations in Table 1 reflect a broad overview of the compositions and P-T conditions observed in Tibet. The goal of this is make the models as realistic as possible. For example, temperatures of 1100°C in the crust are associated with a "magmatically elevated geotherm" [*Hacker et al*., 2000] that can be characterized by emplacement of mantle derived magma in the crust resulting in the generation of hybrid crustal melts [*Annen and Sparks*, 2002]. Moreover, since a pressure of 1 GPa is considered here as the maximum pressure associated with dehydration water contents [*Clemens and Vielzeuf*, 1987], the resulting conductivity estimates will mainly define an upper limit in melt conductivity for those conditions. As seen in Table 1, each water content is associated with a potential source rock for the magma and it is assumed that with increasing temperature the deeper source rocks will be more mafic, involving mainly hornblende dehydration in the water content of the melt.

With the wide variety of P-T conditions involved, the predicted melt conductivities are relatively scattered, with most values in the range 0.1–4 S/m. However, despite a few exceptions, it is worth noting that melt conductivities are generally below the range 3–10 S/m used in previous studies. This point is particularly important, since it shows the substantial impact of a case-by-case constraint of melt conductivity by temperature, pressure, water content, and melt composition. Based on the estimates from Table 1, a maximum melt conductivity value was chosen for each area of interest in order to establish a lower boundary on the melt fraction required to explain the resistivity observed in each area. Assuming contamination of the Songpan-Ganzi crust with more mafic mantle melts, a maximum melt conductivity of 4 S/m has been assumed for the area. For the Kunlun crust, a melt conductivity of 2 S/m appears to be directly linked to the melting of pelitic rocks under relatively low temperatures [*Wang et al*., 2012] (Table 1).

3. Estimation of Melt Fractions Based on MT Resistivity Models

3.1. Crustal Conductance in Northern Tibet

Although MT models are almost always described by resistivity (conductivity) values, the conductance (depth-integrated conductivity) of a conducting layer in the models is much better constrained by MT data

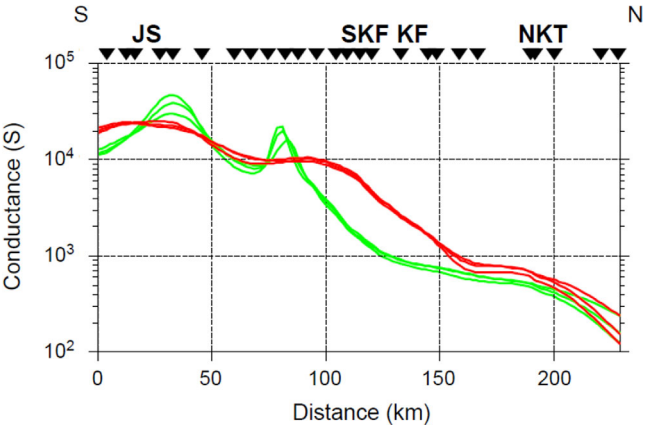

Figure 3. Conductance (20–70 km) derived from 2-D anisotropic inversion of the INDEPTH III profile [*Le Pape et al*., 2012]. The xx (green) and yy (red) values show conductances derived from electric current flow across-profile and along-profile, respectively. For each direction, several models of different smoothness have been evaluated. JS = Jinsha Suture, SKF = South Kunlun Fault, KF= Kunlun Fault, and NKT = North Kunlun Fault.

[*Jones*, 1992]. The conductance of a layer is expressed in Siemens (S), and is defined as the integral of conductivity with respect to depth. For a uniform layer with conductivity σ and thickness h, the conductance S can be expressed as $S = \sigma h$. In magnetotellurics, it can be difficult to define the depth extent of a conductor, since the MT method is mainly sensitive to the depth to the top of the conductive layer and its total conductance rather than its thickness; this is true of all inductive EM methods. As a consequence, estimation of the conductance associated with a particular conductive anomaly is not straightforward, especially as the forward problem is highly nonlinear. Since the crustal conductivity anomaly in northern Tibet evolves into a more complex pattern in the Kunlun area [*Le Pape et al*., 2012], both 2-D anisotropic models of the INDEPTH III data [*Le Pape et al*., 2012], as well as the 3-D models including both INDEPTH III and IV transects [*Wei et al*., 2014], were used to determine robust conductance values for both the Songpan-Ganzi and the Kunlun crust. In order to constrain the conductance of the crustal conductive anomaly defined by the different inversion models, it was assumed that most of the melt responsible for the anomaly was located in the crust. This assumption is based on the observation that temperatures high enough to generate partial melt are known to occur in the crust [*Hacker et al*., 2000; *Mechie et al*., 2004; *Klemperer*, 2006; *Wang et al*., 2012]. It was also based on the fact that partial melting of the crust is known to be widespread on the Tibetan crust [*Wei et al*., 2007]. Hence, the crustal conductance for each 2-D and 3-D model was integrated over the depth range 20–70 km. The upper limit of 20 km was chosen as being the depth above which temperatures are too low for crustal melting [*Mechie et al*., 2004]. The lower limit of 70 km was taken from the average Moho depth in northern Tibet [*Vergne et al*., 2002; *Karplus et al*., 2011]. For the 2-D anisotropic case, in order to get a better estimate of the conductance between those depths, a tear zone [*Mackie*, 2002] was included between 20 and 70 km. The tear zone allows for sharp resistivity contrasts on the upper and lower boundaries, thereby limiting the downward smearing of the conductive layer into the more resistive upper mantle. The final RMS misfits associated with those alternative MT models are similar to the RMS of the original models of *Le Pape et al*. [2012], although slightly lower due to the rougher model permitted by the inclusion of the tear zone. The integrated conductances of the 20–70 km layer were evaluated for several 2-D anisotropic models of different smoothness values in order to check for the consistency in the conductance estimations (Figure 3). On Figure 3, the *xx* and *yy* conductance values represent the horizontal direction for the electrical anisotropy described in *Le Pape et al*. [2012], with *xx* parallel to the strike of the Kunlun Fault, and *yy* perpendicular to the strike of the fault. Whereas the conductance is fairly isotropic in the Songpan-Ganzi terrane, the split between the *xx* and *yy* conductances increases to the north, with the *yy* direction showing higher conductance values associated with the extension of the conductive anomaly to the north (Figure 3). It is worth noting the consistency between the conductances obtained from models derived using different degrees of spatial smoothness (Tikhonov trade-off parameter in the regularized inversions), since it reveals the robustness of the main conductive features in the models. For instance, the conductance of the anisotropic section beneath the Kunlun system appears to be quite well constrained.

For the 3-D case, the constraint that the conductive anomaly be located within the crust was implemented with the use of an a priori model, as used to obtain model 2 in *Wei et al*. [2014]. The conductance values associated with the 3-D model give an alternate estimate to that derived from the 2-D results. For instance, as seen on Figure 4 an east-west conductance profile can be extracted for the two areas of interest. It is however crucial to keep in mind that station coverage is quite limited in the 3-D model, and the conductance values must be used with due consideration. Consequently, both site spacing and consistency in

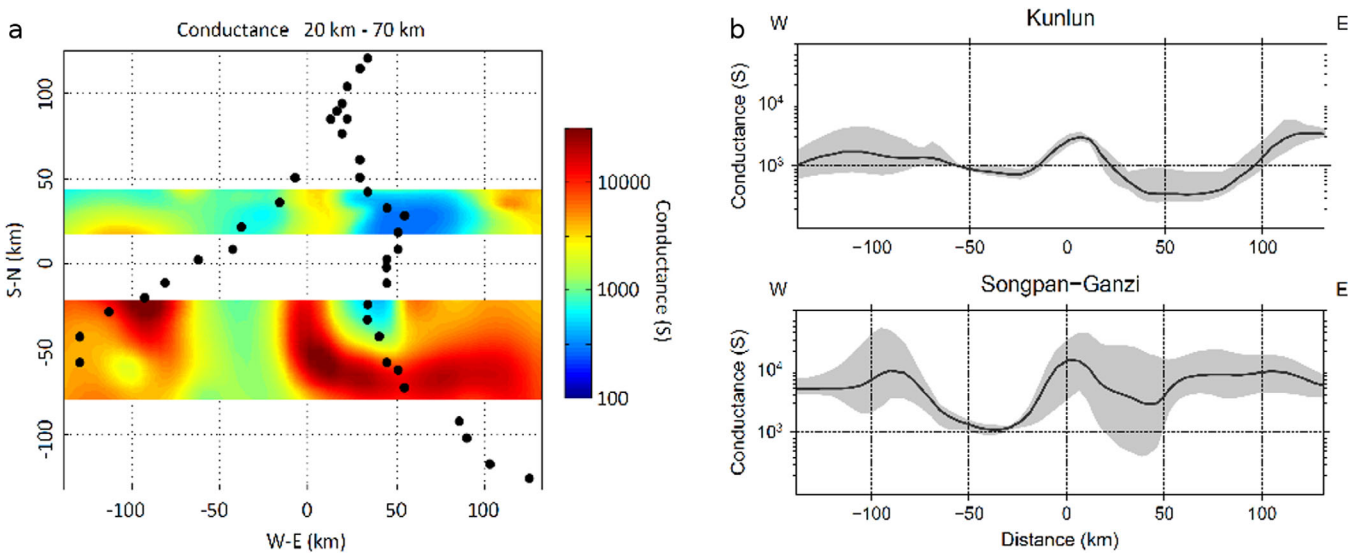

Figure 4. (a) Map of conductance (20–70 km) derived from 3-D resistivity model (model 2 from *Wei et al.* [2014]). Two zones characterizing the Kunlun Fault and Songpan-Ganzi areas are highlighted and E-W conductance profile has been derived. (b) Conductance profiles: the gray area represents the variation in conductance for each area. The black line represents the median values of the conductances for each area.

conductance variations were taken into account when selecting a conductance value from the 3-D model to characterize each area of interest. The comparison of both the 2-D (Figure 3) and 3-D (Figure 4) approaches leads to conductance values in the range 8000–15,000 S for the Songpan-Ganzi crust (between depths of 20–70 km), which are quite consistent with previous studies by *Rippe and Unsworth* [2010] and *Bai et al.* [2010]. The same approach gives a conductance range of 1000–3000 S for the Kunlun crust.

3.2. Melt Quantification

Following a similar approach to *Li et al.* [2003], *Rippe and Unsworth* [2010], and *Bai et al.* [2010], melt fractions were derived from the observed conductance of a particular crustal layer. This is more reliable than using the conductivity of the layer, which is less well determined than the conductance. Since a range of thicknesses must be considered, this will result in a range of melt fractions. In order to convert the observed conductances into melt fractions, several two-phase models were used:

1. The parallel model [*Yu et al.*, 1997; *Roberts and Tyburczy*, 1999] represents a simple two-phase model that is described by conductive layers embedded in a more resistive medium and where the main electric current flow is parallel to the layers. In the case of a partially molten rock, the parallel model is defined as:

$$\sigma_{eff}^{Parallel} = \Phi\sigma_m + (1-\Phi)\sigma_s, \tag{1}$$

   with σ_{eff} the effective conductivity, Φ the melt fraction, σ_s the solid phase conductivity, and σ_m the melt phase conductivity. The solid phase σ_s was set to a value of 0.001 S/m (resistivity of 1000 Ω.m) corresponding to a higher bound for the conductivity of dry lower crustal rocks without interconnected high conductive phases [*Kariya and Shankland*, 1983].
2. The Hashin-Shtrikman upper bound (HS+) [*Hashin and Shtrikman*, 1962] can be modeled as resistive grains inclusions in a conductive melt phase medium [*ten Grotenhuis et al.*, 2005] allowing for complete interconnectivity of the melt phase. The Hashin-Shtrikman upper bound is defined as:

$$\sigma_{eff}^{HS+} = \sigma_m + \frac{(1-\Phi)}{1/(\sigma_s-\sigma_m)+\Phi/3\sigma_m}, \tag{2}$$

   where σ_{eff} is the effective conductivity, Φ is the melt fraction, σ_s is the solid phase conductivity set to 0.001 S/m, and σ_m is the melt phase conductivity.

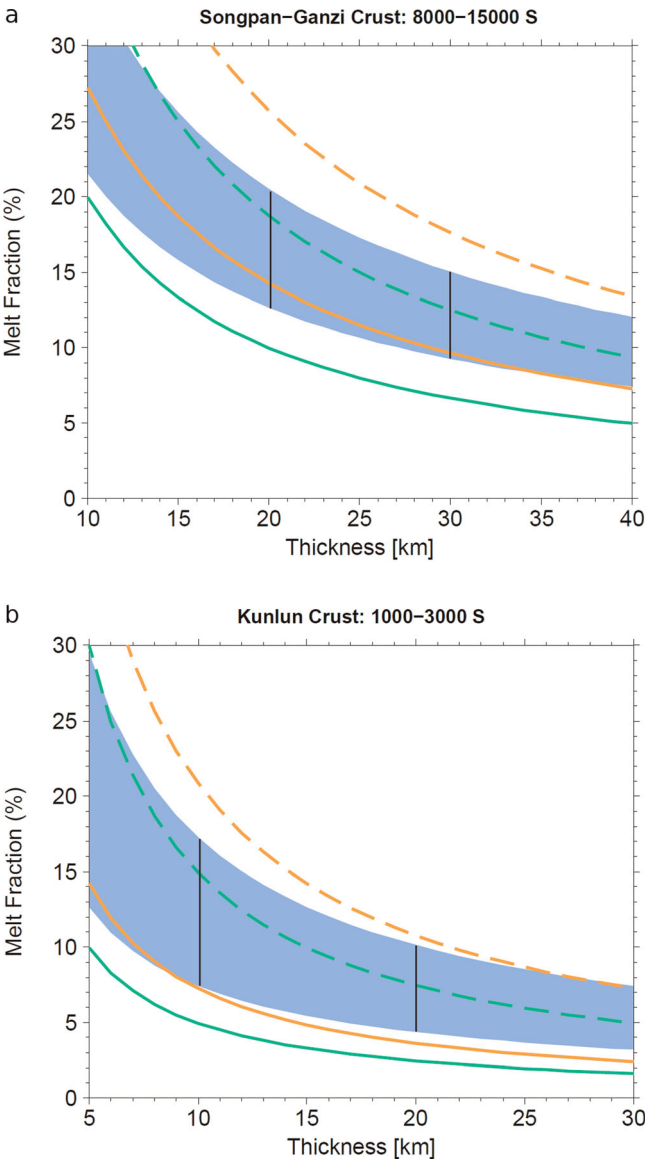

Figure 5. Melt fractions estimated from the Hashin-Shtrikman upper bound (HS+) model (orange), the parallel model (green), and the Archie's Law (blue) for different conductance values. Archie's law being the preferred model, only full and dashed lines are used to represent the outer bounds of the melt fraction estimations based on HS+ and parallel models. (a) Melt fractions for the Songpan-Ganzi terrane associated with thickness 20–30 km using a melt conductivity of 4 S/m. (b) Melt fractions for the Kunlun crust estimated for thickness 10–20 km using a melt conductivity of 2 S/m.

3. The modified Archie's law [*ten Grotenhuis et al*., 2005] is independent of the solid matrix conductivity and the melt connectivity changes with melt fractions [*Watanabe and Kurita*, 1993]. It can be expressed as:

$$\sigma_{eff}^{Archie} = C\Phi^n \sigma_m, \quad (3)$$

where σ_{eff} is the effective conductivity, Φ is the melt fraction, C is Archie's law empirical coefficient, and n is also Archie's law empirical coefficient. For low melt fractions, *ten Grotenhuis et al*. [2005] estimated the effective conductivity to be best described for values of C = 1.47 and n = 1.3.

For each model, the input is the effective conductivity σ_{eff} that is determined from the MT models. Using an estimate of melt conductivity, the melt fraction Φ can be derived from the effective conductivity σ_{eff} assuming good interconnection of the melt phase, which is likely even for low melt fractions [*Partzsch et al*., 2000]. As estimated previously, melt conductivity values of 4 and 2 S/m were used for the Songpan-Ganzi and Kunlun crusts, respectively.

The bulk conductivity σ_{eff} of a two-phase media can be derived directly from the conductance for a fixed layer thickness. Therefore, using different thicknesses for the crustal conductor will give a range of melt fractions (Figure 5). As seen in Figure 5, the modified Archie's law [*ten Grotenhuis et al*., 2005], also used by *Rippe and Unsworth* [2010] and *Bai et al*. [2010], appears to lean toward either the HS+ model or the parallel model depending on the melt fraction. As a consequence, Archie's law (Figure 5, blue swaths) was chosen as the most appropriate model for estimations of the melt fractions as a function of the thickness of the crustal conductive layer. In addition, recent numerical simulations of two-phase random rocks demonstrate that Archie's Law provides an excellent description of bulk conductivity for rocks with melt fractions of 5–30% [*Mandolesi et al*., 2014].

The conductance values used were in the range 8000–15,000 S for the Songpan-Ganzi crustal anomaly and 1000–3000 S for the Kunlun anomaly. For the Songpan-Ganzi crust, other geophysical data can be used to reduce the range of possible thickness for the conductive layer. A thickness in the range 20–30 km is suggested by seismic studies, including *Owens and Zandt* [1997], *Agius and Lebedev* [2014], *Karplus et al*. [2011], and *Yang et al*. [2012]. For the Kunlun crust, the thickness of the layer can be constrained to be in the range 10–20 km based on seismic results [*Karplus et al*., 2011] and is consistent with the channel flow model of

Medvedev and Beaumont [2006]. In summary, the melt fractions inferred for the middle-to-lower crust of the Songpan-Ganzi terrane are in the range 10–21%, which is similar to values reported elsewhere in Tibet by *Rippe and Unsworth* [2010] and *Bai et al*. [2010]. In the Kunlun fault area, estimated melt fractions are inferred to be in the range 5–17%. As shown in Figure 5, several intervals of melt fractions associated with different thickness are highlighted.

3.3. Discussion of Melt Fractions Estimated From MT and Seismic Studies

Although both the elastic and electric properties are sensitive to the presence of partial melt, it is important to note that the two properties do not always exhibit similar sensitivities. In a study of a large magma body in the Central Andes, *Comeau et al*. [2015] showed that seismic and MT derived melt fractions were both in the range 10–20%. However melt fractions estimated with the two techniques are not always in agreement and seismic studies in Tibet have generally given lower estimates of melt fractions compared to those derived from MT studies, such as this study. For instance, *Agius and Lebedev* [2014] estimated melt fractions of 1–2% in the crust of the Qiangtang terrane, consistent with the analysis of *Hacker et al*. [2014], and 3–5% in the Songpan-Ganzi terrane. It should be emphasized that there is a significant difference in the melt fractions estimated for the study area from MT and seismic data. How could these values be reconciled?

In general, seismic velocities, although sensitive to melt fractions, will also be affected by microstructures as well as the whole rock composition [*Christensen and Mooney*, 1995; *Mueller and Massonne*, 2001; *Taylor and Singh*, 2002]. The geometry of melt inclusions can also have a significant impact on seismic velocities [*Schmeling*, 1985; *Takei*, 2000; *Taylor and Singh*, 2002]. The resistivity of partially molten rocks depends strongly on the melt fraction, the degree of interconnection (interconnected melt network versus isolated pocket) [*Partzsch et al*., 2000] and the chemical composition of the melt, especially the water and sodium concentrations [*Gaillard and Marziano*, 2005]. Compared to seismic velocities, electrical resistivities exhibit large variations in the presence of an interconnected conductive phase, making it more sensitive to the melt fractions [*Mueller and Massonne*, 2001; *Schilling and Partzsch*, 2001].

Based on *Takei* [2000] results of melt fraction effects on seismic velocities as a function of the dihedral angle, *Caldwell et al*. [2009] showed that melt fractions estimated from a seismic study in the northwest Himalayas could vary from 7 to 10% with a change in the dihedral angle from 17° to 35°. *Hacker et al*. [2014] also considered the effect of melt geometry on seismic velocities. They reported a decrease of 3% in the shear velocity of the middle crust of the central Qiangtang terrane and by assuming a melt distribution in tubes, they were able to explain this anomaly with a melt fraction that has a lower bound of 2%. Compared to the tube model, the presence of melt in isolated pockets but also in thin films would have lead to higher melt fraction estimates [*Schmeling*, 1985; *Hacker et al*., 2014]. Although isolated pockets would not have affected much the resistivity and therefore the melt fractions derived from MT, the presence of thin films represents a perfectly interconnected melt network which will strongly increase the conductivity.

One way to lower the required melt fraction from MT would be to increase the thickness of the conductivity layer for a fixed conductance, but this parameter is relatively well constrained from different seismic observations. However, as illustrated by *Caldwell et al*. [2009], it is worth noting that dispersion curve inversion remains also nonunique and need to find a trade-off between thickness and velocity of a low-velocity layer. Alternatively, if the melt conductivity was higher, a lower melt fraction would also be required. The melt conductivity values used in this study were derived from analysis of igneous rocks in the vicinity of the Kunlun Fault. While these should give the best constraint, it is possible that the igneous rocks mapped at the surface are not entirely representative of the composition of the magma source at depth that is causing the elevated conductivity. This could occur in two distinct ways: (a) the magma body has evolved over time since the eruption of the lavas or (b) the erupted lavas were differentiated from the parent magma during eruption and have a distinct composition. Both are possible scenarios in northern Tibet. Finally, if the water content in the melt was higher than determined for this study, then this would also increase the melt conductivity and lower the required melt fraction.

Deduced from the conductance study of the Songpan-Ganzi crustal conductive anomaly, the lower limit of effective conductivity characteristic of the partially molten area is around 0.25 S/m (4 Ω.m). It can be shown from Archie's law (equation (3)), that reducing the melt fraction to 2% would require raising the melt conductivity value to 27 S/m. Melt fractions of 5% and 10% would, respectively, lead to melt conductivity values of 8 and 3.5 S/m. This shows how having a good constraint on melt conductivity can lead to robust

estimates of melt fractions. A value of 27 S/m for melt conductivity appears to be unrealistic for the temperatures, pressures, and compositions characterizing the area. Furthermore, according to SIGMELTS and Table 1, reaching a melt conductivity value of 8 S/m would require a melt water content higher than 25 wt%. First of all, such value cannot be reached by dehydration melting alone [*Clemens and Vielzeuf*, 1987] and secondly a water content that high would also reach well above water solubility associated with granitic melts [*Holtz et al*., 2001]. The inferred melt fraction estimates from the resistivity models are consistent with values predicted from fluid-absent melting petrological models at the observed P/T conditions and for similar composition. For instance, at 1 GPa and 900°C with presence of 0.6 wt % H_2O in the source rock (in agreement with the mineralogy of Qiangtang defined by *Hacker et al*. [2014]), *Clemens and Vielzeuf* [1987] predicted melt fractions of ~20% for dehydration melting of pelites and quartzofeldspathic rocks, ~15% for dehydration melting of intermediate rocks, and ~10% for dehydration melting of mafic rocks. In addition, the water contents used in our study were taken from *Clemens and Vielzeuf* [1987] and are relatively high estimates. For example, they do not take into account the substitution of OH^- by other component, such as fluorine F^- in natural micas, as observed on xenoliths data from xenoliths data from central Tibet [*Hacker et al*., 2000, 2014]. However, diminishing the water content released from melting of hydrous phases would result in lower melt conductivities and therefore higher melt fractions.

For all the reasons described above, we believed that our melt fraction estimates are robust although they remain higher than those derived from the seismic studies of *Agius and Lebedev* [2014] and *Hacker et al*. [2014].

4. Flow Characterization

In the previous section, the MT inversion models were used to estimate the amount of melt in the crust of Northern Tibet. In this section, we define flow patterns for the area of interest. In order to constrain geodynamic models, we need to develop a link between the rock strength and the melt fraction, and two complementary methods are used. Method A uses a range of laboratory studies on the rheology of partially molten rocks without any constraint on temperature, and method B uses an empirical flow law to introduce temperature as an additional constraint.

4.1. Defining the Flow Pattern

Channel flow in the partially molten crust of Tibet has been previously described as a combination of Couette flow and Poiseuille flow [*Grujic*, 2006; *Klemperer*, 2006; *Rippe and Unsworth*, 2010]. Couette flow is the laminar flow of a viscous fluid in the space between two parallel plates, which are moving relative to each other. Poiseuille flow is pressure-induced flow (channel flow) in a layer, usually a pipe, and is distinct from drag-induced flow such as Couette Flow (Figure 6). Calculating the possible Poiseuille flow velocity and Couette flow velocity is important to determine which type of flow dominates. For instance, if Poiseuille flow is dominant, topography-driven channel injection in the transition zone defining the northern margin of the plateau becomes possible. Although the average Couette flow velocity is defined as half of the velocity of the dragging layer, Poiseuille velocity will depend on additional parameters as described below.

A one-dimensional "layer-type" flow was used to model Poiseuille flow velocities in the Songpan-Ganzi crust (Figure 6). However, in order to reflect the complexity of the flow across the Kunlun fault revealed by the recent magnetotelluric studies [*Le Pape et al*., 2012; *Wei et al*., 2014], the layer model was replaced by a "pipe-type" flow model (Figure 6) [*Turcotte and Schubert*, 2014]. Hence, in this paper, the layer model will be associated with the term "Songpan-Ganzi flow," whereas the term "Kunlun flow" will be related to the pipe flow model. For consistency with the study of *Rippe and Unsworth* [2010], the power law associated with non-Newtonian fluids ($n > 1$ in equation (4)) is defined in a similar manner in order to introduce also the material constant A_{eff} (equation (4)).

$$\sigma^n = A_{eff}\dot{\epsilon}. \tag{4}$$

It should be noted that in this discussion of flow the variable σ is associated with stress and not electrical conductivity. The average velocity of the Poiseuille flow ($\bar{u}$) as well as its flux (Q) can be expressed as a function of the pressure gradient (dP/dx) along the flow direction and the material constant (A_{eff}) for both type of flow described above [*Rippe and Unsworth*, 2010; *Turcotte and Schubert*, 2014]. For a layer thickness h, $\bar{u}_{layer}$ and Q_{layer} are then defined as:

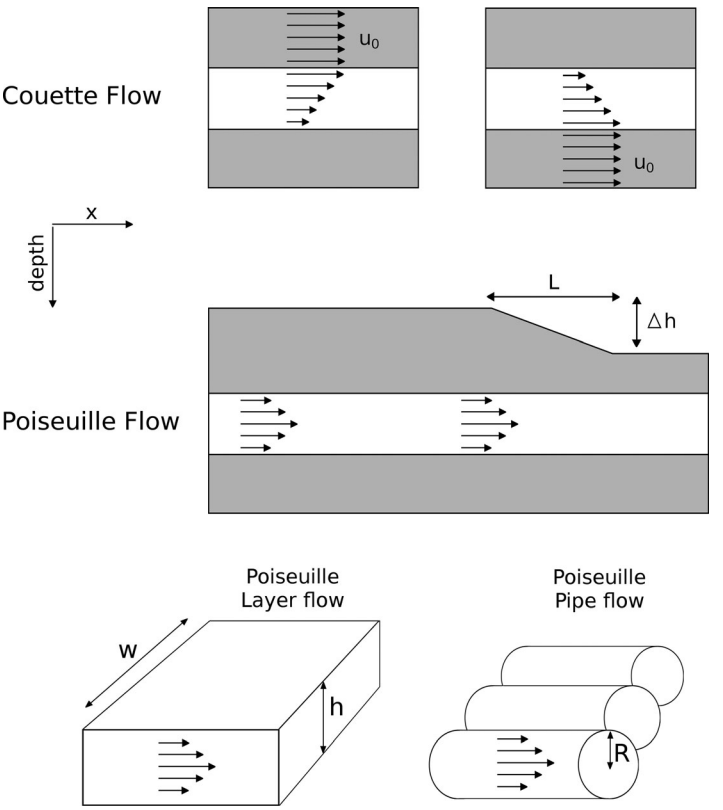

Figure 6. Schematic representation of the channel flow models: Couette flow is induced by relative motion of its bounding layers. Poiseuille flow is driven by pressure gradient associated with topography variations. In this study, two types of models are considered for calculating Poiseuille flow velocities: layer flow model and pipe flow model.

$$\bar{u}_{layer} = \frac{(dP/dx)^n h^{n+1}}{2^{n+1}(n+2)A_{eff}} \quad (5)$$

and

$$Q_{layer} = \frac{(dP/dx)^n h^{n+2}}{2^{n+1}(n+2)A_{eff}}. \quad (6)$$

As mentioned previously, as the flow appears more spatially heterogeneous further north it is modeled as pipes. The introduction of this type of flow not only keeps the problem relatively simple but also introduces extra lateral constraints to the flow. The effects of the number of pipes are also discussed further in the paper. For a pipe radius R, $\bar{u}_{pipe}$ and Q_{pipe} along the pipe can be expressed as [*Turcotte and Schubert*, 2014]:

$$\bar{u}_{pipe} = \frac{(dP/dx)^n R^{n+1}}{2^n(n+3)A_{eff}} \quad (7)$$

and

$$Q_{pipe} = \frac{\pi(dP/dx)^n R^{n+3}}{2^n(n+3)A_{eff}}. \quad (8)$$

4.2. Method A: No Temperature Included, Rheology Based on Several Laboratory Studies

Rippe and Unsworth [2010] discussed flow velocity variations as a function of the vertically integrated conductance by fixing either the bulk electrical conductivity or the thickness of the channel. Compared to conductance, melt fractions are directly linked to stress and then flow velocity. Therefore, as an alternative to *Rippe and Unsworth* [2010], the method presented here aims at expressing the flow velocity as a direct function of melt fractions based on the determination of the material constant A_{eff} from different laboratory measurements.

A broader variety of laboratory studies [*Arzi*, 1978; *van der Molen and Patterson*, 1979; *Rushmer*, 1995; *Rutter and Neumann*, 1995] were also taken into account in order to check for consistency and introduce results from different conditions and compositions. Those particular studies were considered since the associated laboratory measurements were performed on rocks with low melt fractions. *Arzi* [1978] reported measurements for relative viscosities on Westerly granites with melt fractions ranging from 6 to 17%, respectively, associated with temperatures of 860°C and 1020°C. *van der Molen and Patterson* [1979] presented results on relative viscosity for partially melted granite (delegate aplite) with melt fractions of 5–25% at temperature of 800°C and at a confining pressure of 300 MPa. As an alternative, the results from *Rushmer* [1995] show the effects of low melt fraction (<20%) on viscosity for partially molten amphibolites. The later experiments were carried out at temperatures ranging from 650°C to 1000°C and at pressures of 1.8 GPa. This last study is particularly interesting since it considers a more mafic composition and considers conditions that occur in the lower part of thickened lower continental crust. Finally, *Rutter and Neumann* [1995] also studied the rheological behavior of the Westerly granites with melt fractions ranging from 3% at 800°C to 50% at 1000°C at a confining pressure of 250 MPa. Since those measurements only reflect rheological behavior of the samples for a few melt fractions, *Rosenberg and Handy* [2005] and *Costa et al.* [2009] interpolated and extrapolated the results through two different models in order to reconstruct the rheological behavior of the laboratory samples for a broader range of melt fractions. Where *Rosenberg and Handy* [2005] focused

on low melt fractions, the *Costa et al*. [2009] model can be applied to a wider range of fractions and is more adapted for low to intermediate ranges (20–70%). However, the *Costa et al*. [2009] model is only used here for relatively low melt fractions and therefore the results presented here were mainly constrained by laboratory measurements made for lower fractions. The parameters used for the model for each type of samples are described in *Costa et al*. [2009]. Figure 7a summarizes the rheology used in method A.

A range of methods can be used to derive a single equation from a set of scattered data points such as those shown in Figure 7a. Whereas the *Rosenberg and Handy* [2005] models are least squares-exponential fits to the laboratory data, the *Costa et al*. [2009] model represents a semiempirical law expressing the relative viscosity as a function of crystal fraction (or melt fraction) as well as several other empirical parameters characteristic of the type of samples used to calibrate the model. Finally, one interesting point is that the two models both extrapolated the results on granites of the *Rutter and Neumann* [1995] and van der *Molen and Patterson* [1979] studies, which is very useful for scaling/consistency checks. As a matter of fact, as seen in Figure 7a, the results from both models that are based on *Rutter and Neumann* [1995] samples show very good agreement for melt fraction above 5%. For the van der *Molen and Patterson* [1979] samples, the fit between the two models is not in such agreement. Furthermore, *Costa et al*. [2009] also highlighted there are some uncertainties on the measurements from *Arzi* [1978] and *Rutter and Neumann* [1995].

The material constant A_{eff} can be derived from the different laboratory studies presented above and can be expressed as a function of partial melt fraction (Figure 7a). Accordingly, the Poiseuille flow velocity can be determined as a function of partial melt following the equations described above. In order to remain consistent with *Rippe and Unsworth*'s [2010] approach, a power-law exponent of $n = 3$ was chosen to be used with method A. Finally, it was decided to consider all models presented on Figure 7a for velocity calculations in order to establish upper and lower boundaries in the flow constraints discussed further.

4.3. Method B: Including Temperature Effects

Deformation rates used in the laboratory are many orders of magnitude higher than those encountered in the Earth [*Jamieson et al*., 2011]. This means that extrapolation of laboratory results to geological studies must be done with due care. This is one of the main reasons for introduction of method B for comparison and robustness improvement in the observations. Furthermore, in contrast with method A, this method enables the introduction of a crucial parameter to the problem; namely temperature. *Rutter et al*. [2006] derived a flow law (equation (9)) for describing the rheological behavior of partially molten granites.

$$\dot{\epsilon} = A\sigma^n exp(B\Phi^m) exp(-H/RT). \tag{9}$$

This empirical equation was derived to fit rheological measurements on synthetic wet (2.5 wt % water) partially molten granites with relatively low melt fractions (10–30%) for temperatures ranging from 900°C to 1000°C. Those settings appeared to fit quite well with the conditions associated with this study. Since method A is restricted by higher strain rates typical of laboratory measurements, it is important to use a different approach where the extrapolation of the strain rates can be made directly through a flow law.

The parameters of equation (9) were obtained by *Rutter et al*. [2006] through linear regression and are defined such as $\log(A) = -1.39$, $m = 2$, $n = 1.8$, $B = 192$, and $H = 220 \pm 65$ kJmol^{-1}, Φ is the melt fraction (<1), and T is the temperature (K). The values of m are not well constrained and likely range between 2 and 3.5, but the authors considered a value of $m=3$. In this study, a value of $m = 2$ was adopted in order to increase the impact of lower melt fractions in the flow law and thus to obtain a minimum boundary on melt fractions associated with significant strength drop. Despite being based on laboratory studies, *Rutter et al*. [2006] extrapolated the relation of equation (9) for lower or geological strain rates for investigating the extremely weak rheological behavior of migmatitic granitic melt. Furthermore, the method has also proven to be relevant for defining constraints on the viscosity of the partially molten midcrust in Tibet [*Rutter et al*., 2011]. The use of the flow law enables the introduction of the dependence on temperature and melt of the material constant in a direct relationship (equation (9)). Figure 7b summarizes the rheology used in method B.

It is worth noting that in equation (9) the power law is characterized by a value of $n = 1.8$, which is lower than the value considered in method A. Figure 7b presents the rheology associated with method B for values of $n = 1.8$ but also uses $n = 3$ for comparison with the rheology used in Method A. For a value of $n = 3$, both methods appear to give relatively consistent results. Figure 7b also clearly shows how the drop in strength associated with a critical melt fraction diminishes as the temperature increases. *Grujic* [2006]

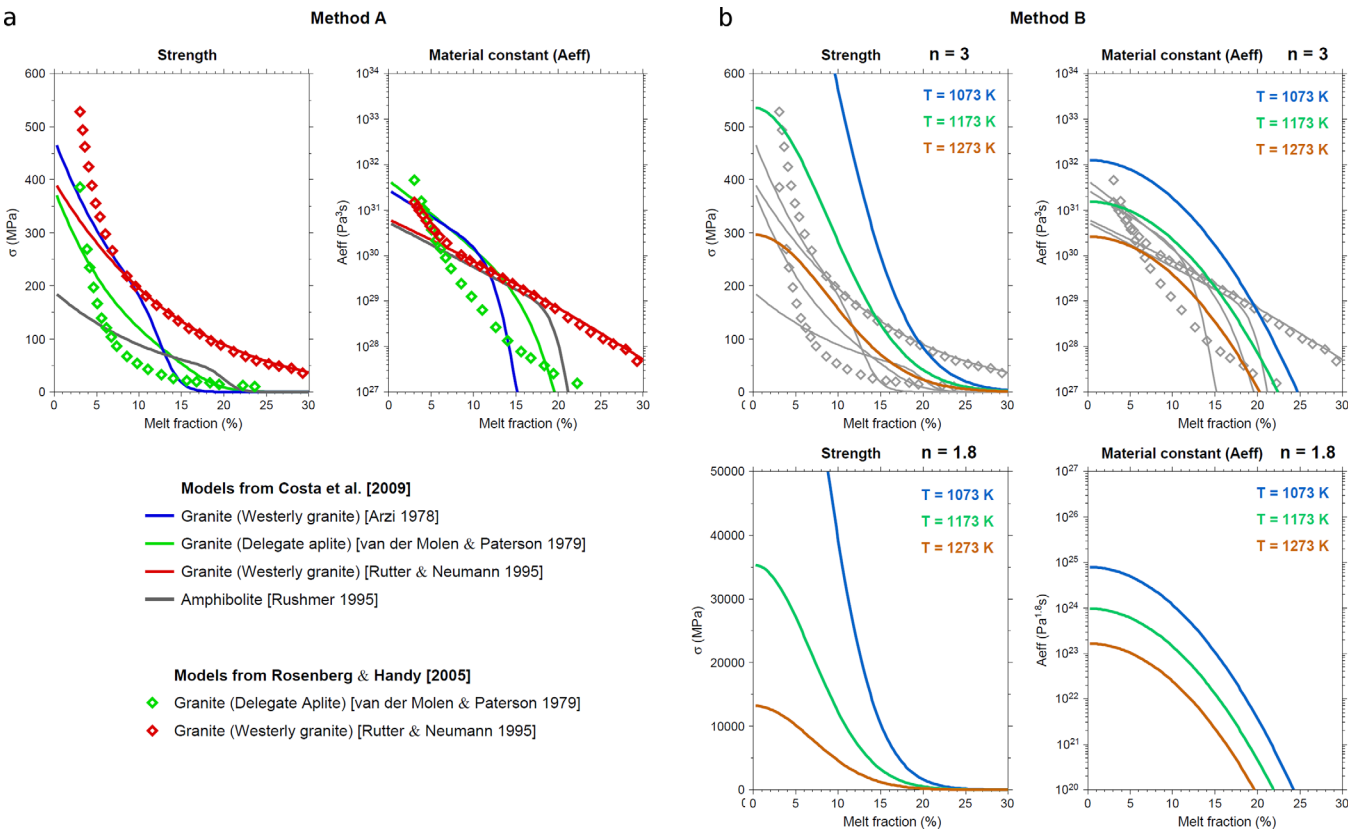

Figure 7. (a) Rheology of Method A: Strength and material constant as a function of melt fractions derived from different laboratory studies and summarized by *Rosenberg and Handy* [2005] and *Costa et al.* [2009]. (b) Rheology of Method B: Strength and material constant as a function of melt fractions derived from equation (9) (including grain size rescaling) [*Rutter et al.*, 2011]. Whereas a stress exponent of n = 1.8 is used for the power law in this study, an exponent of n = 3 was also considered for a direct comparison with the rheology used in method A (plotted in gray).

highlighted that having a lower stress exponent in the power law (n = 1.8 instead of n = 3) lowers the relatively high dependence of the effective viscosity on stress and brings more weight on the effect of temperature. This is particularly a key point to consider in the further discussion on the initiation of channel flow, since it shows that methods A and B do not show the same dependence on stress.

Finally, *Rutter et al.* [2006] mentioned that as the strain rate or flow stress decreases, the stress exponent n is likely to decrease. Therefore, the strain rates predicted by equation (9) can be considered as upper bounds. Equation (9) was determined for a grain size of 50 μm, and, based on a study on viscosity of basaltic melts, *Scott and Kohlstedt* [2006] showed that the flow rate will tend to decrease with increasing grain size. Therefore, in their study on crustal viscosity in Tibet *Rutter et al.* [2011] rescaled the flow law (equation (9)) to larger grain size of 0.5 mm in order to obtain what they considered would be a better representation of lower crustal partially molten rocks. The exact same correction to the flow law was adopted in this study. Finally, one parameter not taken into account in method B is the variation in the melt water content and how that will affect viscosity: water content in the melt will have a significant impact on rock viscosity [*Hess and Dingwell*, 1996; *Pommier et al.*, 2013]. Furthermore, *Mecklenburgh and Rutter* [2003] defined, through an empirical law, that the activation enthalpy in a partially molten granite is mainly dependent on the melt water content. Based on Table 1 results for water content estimates in the melt, we can assume in this study that the water content of 2.5 wt % used for *Rutter et al.* [2006] calculations would define once again an upper bound on the strain rates associated with equation (9).

4.4. Effective Viscosity and Consistency Check on Melt Fraction Estimates

In order to further discuss the melt fractions estimated from the MT results in Figure 5, melt fractions are estimated directly from the published viscosity estimates of *Ryder et al.* [2011] using the equations previously introduced in both methods A and B. *Ryder et al.* [2011] used a heterogeneous viscosity model

characterized by steady state viscosities of 10^{19} Pa.s beneath the north of the Songpan-Ganzi terrane and 4.10^{19} Pa.s beneath the southern boundary of the Qaidam basin in order to fit GPS time series in the Kunlun fault area. Those values were considered to define an effective viscosity characteristic of both Sonpgan-Ganzi (10^{19} Pa.s) and Kunlun (4.10^{19} Pa.s) flows. The higher viscosities in the Kunlun area would therefore also highlight the more complex pattern in melt distribution [*Le Pape et al*., 2012; *Wei et al*., 2014].

For method A, the effective viscosity and the material constant can be related through the following equation presented in *Rippe and Unsworth* [2010]:

$$\eta_{eff} = \frac{1}{2}(A_{eff})^{1/n}\dot{\epsilon}^{(1/n)-1}. \tag{10}$$

Since the material constant (A_{eff}) was previously expressed as a function of melt fractions (Figure 7a), the latter can be related to effective viscosity through relation equation (10). By considering the range of laboratory studies shown on Figure 7a, maximum and minimum melt fractions can be estimated for different strain rates associated with a single value of effective viscosity characteristic of each area of interest (Figure 8a). Strain rates in the range 10–20 nanostrain.yr^{-1} (Figure 8a, $10^{-15.5}$–$10^{-15.2}$ s^{-1}) were proposed for northern Tibet by *Gan et al*. [2007] based on their study of crustal motion and deformation in Tibet based with GPS data. Using these strain rates, melt fractions were estimated in the range 15–36% for the Songpan-Ganzi crust and 9–21% for the Kunlun crust.

For method B, equation (9) shows that the strain rate and stress are directly dependent on melt fraction. Therefore, the calculation to estimate melt fraction is more straightforward than in Method A. In *Rippe and Unsworth* [2010], equation (10) was defined for n values of 2–4; here we are dealing with a value of n = 1.8, therefore, a simpler approximation of the effective viscosity [*Grujic*, 2006; *Turcotte and Schubert*, 2014] is defined as:

$$\eta_{eff} \simeq \sigma/\dot{\epsilon}. \tag{11}$$

The combination of equations (9) and (11) enable estimation of melt fractions as a function of effective viscosity, temperature, and strain rate. The results are presented in Figure 8b. The same strain interval used for method A and described above is considered here. For both the Songpan-Ganzi and Kunlun areas, the temperature range considered was 800 to 1000°C, based on the geotherms presented in Figure 2. For the north Kunlun area, the upper limit higher temperatures of 1000°C are quite high for the area (Figure 2) and could reflect the possibility of strain heating [*Whittington et al*., 2009]. The melt fractions obtained are ~18% at 800°C, ~15% at 900°C, and ~12% at 1000°C for the Songpan-Ganzi crust, and ~14% at 800°C, ~10% at 900°C, and 4–7% at 1000°C for the Kunlun crust. Consequently, these results confirm that for a fixed viscosity value, less melt is required at higher temperatures.

A comparison of the melt fractions estimates from methods A and B, as well as with the estimates based on conductances, is shown in Table 2. It is reassuring to see that the estimates are in fairly good agreement with each other following three different approaches; this brings further robustness in the defined interval of melt fractions for both investigated areas. Furthermore, the results based on viscosity are used to constrain an upper limit in the melt fraction. In the following discussion, melt fractions of 18% and 14% for the Songpan-Ganzi and Kunlun crust, respectively, will be considered as maximum estimates. Finally, it is also worth noting that as an alternative approach, method B could also be used to investigate crustal temperatures in northern Tibet, by using the effective viscosity and melt fraction determined from the resistivity models.

5. Constraints on Channel Flow Occurrence in Northern Tibet

In this section, both methods A and B are used to investigate if topographically driven channel flow occurs in northern Tibet. The average Couette flow velocity can be defined as half the velocity of the dragging plate [*Turcotte and Schubert*, 2014]. Since the convergence rate between underthrusting India and southern Tibet has been estimated as 2 cm/yr [*Ader et al*., 2012], and if we assume that a flow rate on the northern Tibetan boundary is a relatively instantaneous response to the convergence rate on the southern boundary, the average Couette velocity can be taken as 1 cm/yr. For further discussion on the effects of decreasing Couette velocity, a value of 0.5 cm/yr was also considered assuming average Couette flow velocities would be lower in northern Tibet. For a Poiseuille velocity significantly greater than the Couette velocity thresholds, channel flow driven by pressure gradients can be concluded to be the dominant type of crustal flow.

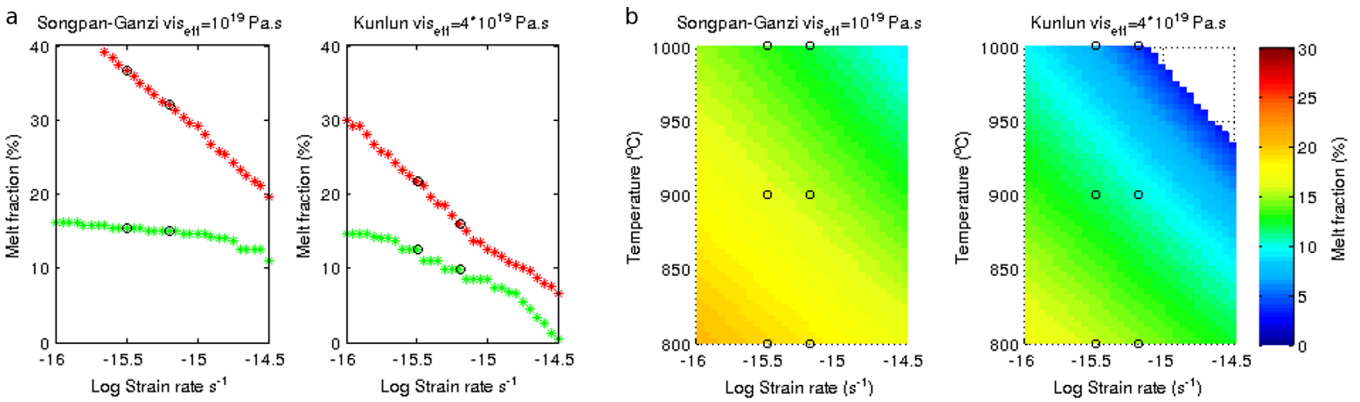

Figure 8. Melt fractions derived from effective viscosity estimates [*Ryder et al.*, 2011] for strain rate interval 10–20 nanostrain.yr^{-1} ($10^{-15.5}$–$10^{-15.2}$ s^{-1}) [*Gan et al.*, 2007]. (a) Upper (red) and lower (green) limits in melt fractions derived from fixed effective viscosity as a function of strain rate using method A. Circles represent melt fractions defined by the strain rate interval for each curve. (b) Melt fractions derived from fixed effective viscosity as a function of temperature and strain rate using method B. Circles represent melt fractions defined by the strain rate interval for 800, 900 and 1000°C.

Different pressure gradients and channel thicknesses (diameters) were tested for the Poiseuille velocity estimations. For each scenario, a melt fraction is associated with the last model to pass above the Couette velocity. Therefore, the minimum melt fraction defines a lower limit for the occurrence of Poiseuille flow.

5.1. Method A Analysis

The different laboratory studies described in method A were used to calculate Poiseuille flow velocities as a function of melt fraction, and results are summarized in Figure 9. For each Couette velocity threshold, a maximum melt fraction can be determined for the last "laboratory-derived" Poiseuille flow velocity to be greater than the Couette threshold. Figure 9 shows the melt fractions for which all laboratory studies are above the Couette thresholds of 1 or 0.5 cm/yr as a function of the thickness of the partially molten layer (Songpan-Ganzi) or pipe diameter (Kunlun), and as a function of lateral pressure gradient.

The lateral pressure gradient is a function of the topographic variation Δh over a distance L (Figure 6) but also depends on crust ρ_c and mantle ρ_m densities. The mantle density $\rho_{m.}$ is defined here as 3300 kg/m^2 [*Medvedev and Beaumont*, 2006; *Rippe and Unsworth*, 2010] and the crust density is defined as 2600 and 2800 kg/m^2 for the Songpan and Kunlun crust, respectively [*Jimenez-Munt et al.*, 2008]. For the Kunlun block, due to the drop in average topography ($\Delta h = 1500$ m) north of the Kunlun fault system over a short distance (L = 100 km), a pressure gradient of 120 Pa/m was considered as a reference for the Kunlun area. For the Songpan-Ganzi terrane, it can be assumed a topographic variation of $\Delta h = 1500$ m with respect to the Qaidam basin over a distance of around L = 200 km. Furthermore, on a broader scale, the eastern part of the high elevated Songpan-Ganzi terrane will have a topographic variation of $\Delta h = 4000$ m with respect to the Sichuan basin over a distance of around L = 500 km. Those two estimations lead to the use of a reference pressure gradient of 80 Pa/m for the Songpan-Ganzi terrane, a value also used by *Rippe and Unsworth* [2010] for central Tibet. However, due to uncertainties on pressure gradient estimations, a broad range of pressure gradients from 70 to 130 Pa/m are considered for comparisons (Figure 9). Following the melt

Table 2. Summary of Melt Fractions Derived From Resistivity and Viscosity for Both Songpan-Ganzi and Kunlun Areas as a Function of Layer Thickness and Temperature

		Songpan-Ganzi			Kunlun		
		20 km	25 km	30 km	10 km	15 km	20 km
Conductance		13%–21%	11%–17%	10%–15%	8%–17%	6%–12%	5%–10%
Viscosity 1			15%–36%			9%–21%	
Viscosity 2	800°C	**~18%**	**~18%**	**~18%**	**~14%**	**~14%**	**~14%**
	900°C	~15%	~15%	~15%	~10%	~10%	~10%
	1000°C	~12%	~12%	~12%	4%–7%	4%–7%	4%–7%

Bold values define the upper limit in melt fractions for each area and are used further for constraints on channel flow.

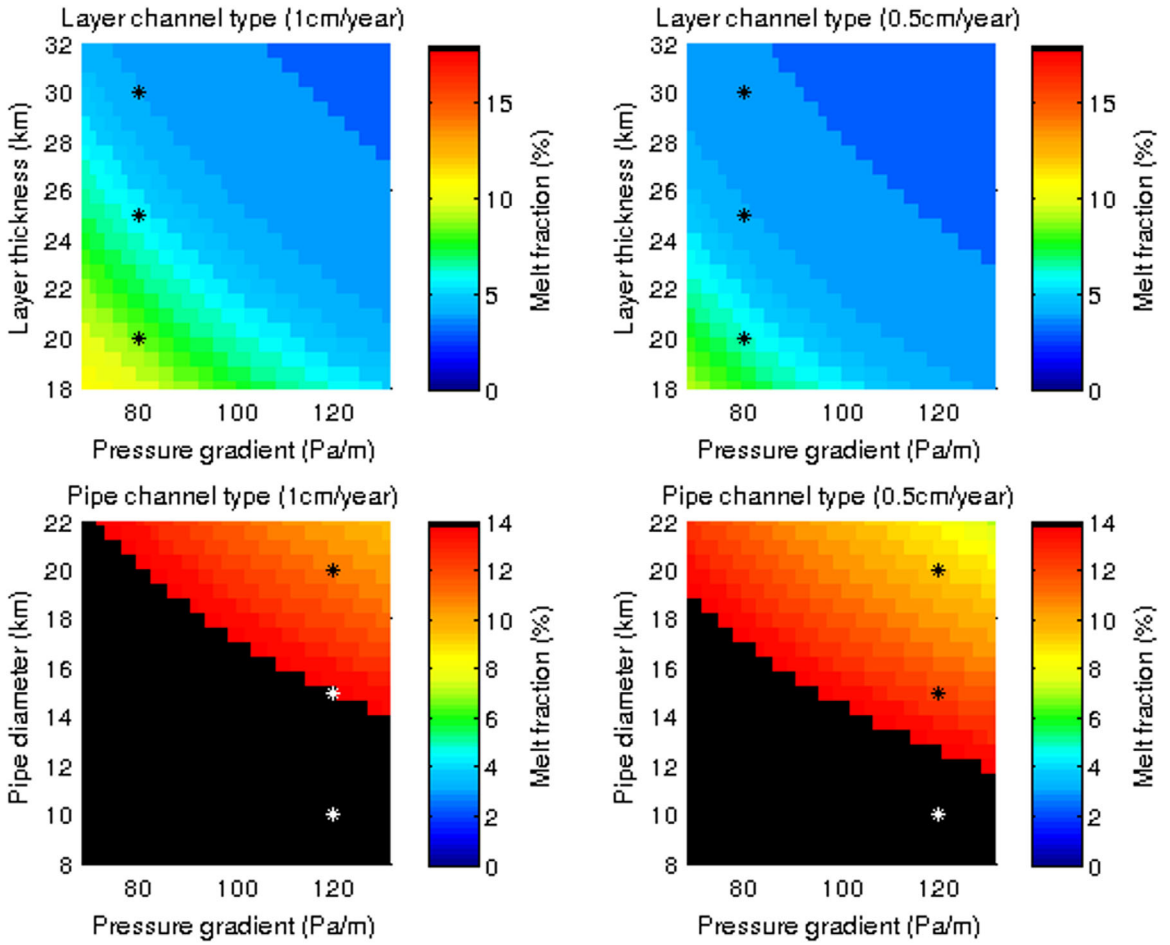

Figure 9. Minimum melt fractions required for Poiseuille flow to dominate, based on method A. The reference pressure gradient of 80 Pa/s is associated with the Sonpgan-Ganzi area (layer model). A reference pressure gradient of 120 Pa/m is defined for the Kunlun area (pipe model) due to the steep decrease in topography further north. The black areas represent the melt fractions above the upper limit determined for the melt fraction in the Songpan-Ganzi (18%) and Kunlun (14%) areas.

fraction study based on resistivity models, the thickness of the layer in the layer model is defined between 20 and 30 km. Similarly, the diameter of the pipe model is defined by values ranging from 10 to 20 km.

For the Songpan-Ganzi area (layer-type), the melt fractions necessary for topography-driven channel flow to occur are plotted in Figure 9 (top plots) and never exceed 10%, which was the melt fraction derived from electrical conductivity (Figure 5) and regional viscosity (Figure 8). Therefore, those observations support the conclusion that topography driven channel flow could occur in the Songpan-Ganzi crust.

However for the Kunlun area (pipe-type), melt fractions in Figure 9 (bottom plots) exceed the maximum values defined for the area (14%) for some combinations of pipe diameter and pressure gradient. First of all, the observations clearly show the substantial impact of the pressure gradient for Poiseuille flow dominance. For instance, if the pressure gradient remains unchanged from the Songpan-Ganzi area, the results highlight that the Poiseuille velocity does not exceed the Couette velocity of 1 cm/year. Second, the diameter of the pipes also has a significant impact on the conditions necessary for topography-driven channel flow to occur. Figure 9 reveals that if the pressure gradient is high enough the Poiseuille flow will remain dominant for a pipe diameters of 20 and 15 km depending on the Couette threshold. However, for pipes with a diameter as low as 10 km, the control of the flow by pressure gradients may not extend to the Kunlun area. Those different observations are intriguing and enable us to place constraints on the evolution of the Poiseuille flow domination further north of the Kunlun fault system.

Let us now consider the exact same problem through method B enabling the introduction of another substantial parameter, and that is temperature.

5.2. Method B Analysis

For method B, a very similar approach as described in method A was followed except here there is only one Poiseuille velocity considered, which is directly derived from equation (9) enabling the introduction of temperature dependence. As seen in Figure 10, this analysis exposes the domination of Poiseuille flow as a function of temperature, layer thickness (or pipe diameter), and pressure gradient. The same Couette velocity thresholds of 1 or 0.5 cm/yr were also used here.

Concerning the layer type model, it appears that for the Couette velocity thresholds considered the maximum melt fraction required for Poiseuille flow to occur is 13% for a temperature of 800°C. This value belongs to the lower bounds of melt fractions characterizing the Songpan-Ganzi area. This result is in good agreement with the results from method A, which is reassuring regarding the robustness of the observations and consistency between methods A and B. The other interesting result brought by method B about the Songpan-Ganzi area is that for temperature of 1000°C, partial melt is not needed for Poiseuille flow to be dominant since at high temperatures dry rocks will undergo creep.

The pipe-type flow model related to the Kunlun area shows that a specific set of conditions is needed for topography driven channel flow to occur. For instance, it appears that temperatures of 800°C are probably too low for the Poiseuille velocities to be dominant. At 900°C, a pipe of 10 km diameter is closer to the limit for permitting topography-driven channel flow. Furthermore, for a pipe of 20 km diameter the maximum melt fraction needed for Poiseuille velocities to be above 1 cm/yr is 10%. This value is in very good agreement with the estimates based on both viscosities from *Ryder et al*. [2011] as well as results from the resistivity study (Figure 5). However, it is worth noting that 10% is the upper limit of the melt fraction interval defined by a 20 km pipe diameter for the Kunlun conductive anomaly. Finally, for temperatures of 1000°C all melt fractions are less than the maximum fraction value of 14% determined for the Kunlun area. Therefore, although a crustal temperature of 1000°C is perhaps unrealistic for this area, channel injection would be possible at this temperature.

Despite being based on an empirical equation, the analysis used in method B gives some very interesting results and highlights the fact that temperature is a parameter as crucial as the melt fractions in differentiating the domination of Couette and Poiseuille flow. For instance, as the temperature increases Poiseuille flow becomes dominant in the Songpan-Ganzi crust regardless of the melt fraction. Furthermore, the results from method A, which are in good agreement with method B, are revealed to be an excellent consistency check. Such agreement is related to the fact that an increase in melt fraction for Method A will also imply an increase in temperature.

In order to summarize the observations, melt fractions derived from Table 2 are presented in Figure 11 where they are compared with the melt fractions thresholds defined above for topography-driven channel flow to occur as a function of channel thickness (or diameter) and temperature. In the Songpan-Ganzi terrane, channel flow could occur in a mid-to-lower crustal layer that was partially molten. For the crust beneath and north of the Kunlun fault, channel flow could occur at temperatures closer to and above 900°C. As seen on Figure 2, *Wang et al*. [2012] predicted that the temperatures associated with the observed felsic rocks along the Kunlun Fault system could be as high as 900°C. For higher temperature to be present in the mid-lower crust, a process such as strain heating [*Whittington et al*., 2009; *Nabelek et al*., 2010] could produce temperature closer to 1000°C, which would lead to Poiseuille flow domination.

6. Proportion of Crustal Flow Injected North

The models proposed by *Clark and Royden* [2000] define crustal flow that is directed to the east, parallel to the strike of the Kunlun Fault. Our analyses presented above support the idea that some crust is injected northward across the Kunlun Fault. Therefore, an important outstanding question is to determine what proportion of the main crustal flow extends to the north.

Let us define Q_{north} as the flux directed north across the Kunlun Fault, Q_{east} as the flux directed east parallel to the Kunlun Fault, and Q the overall flux present in the Songpan-Ganzi block. By assuming conservation of mass, total Q can be defined as: $Q = Q_{north} + Q_{east}$. The proportion of flux directed north can then be expressed as the ratio $F = Q_{north}/Q$. In order to compare the two types of flux Q_{north} and Q, and to evaluate the proportion of crustal flow crossing the Kunlun fault to the north, the flux through a layer of thickness h

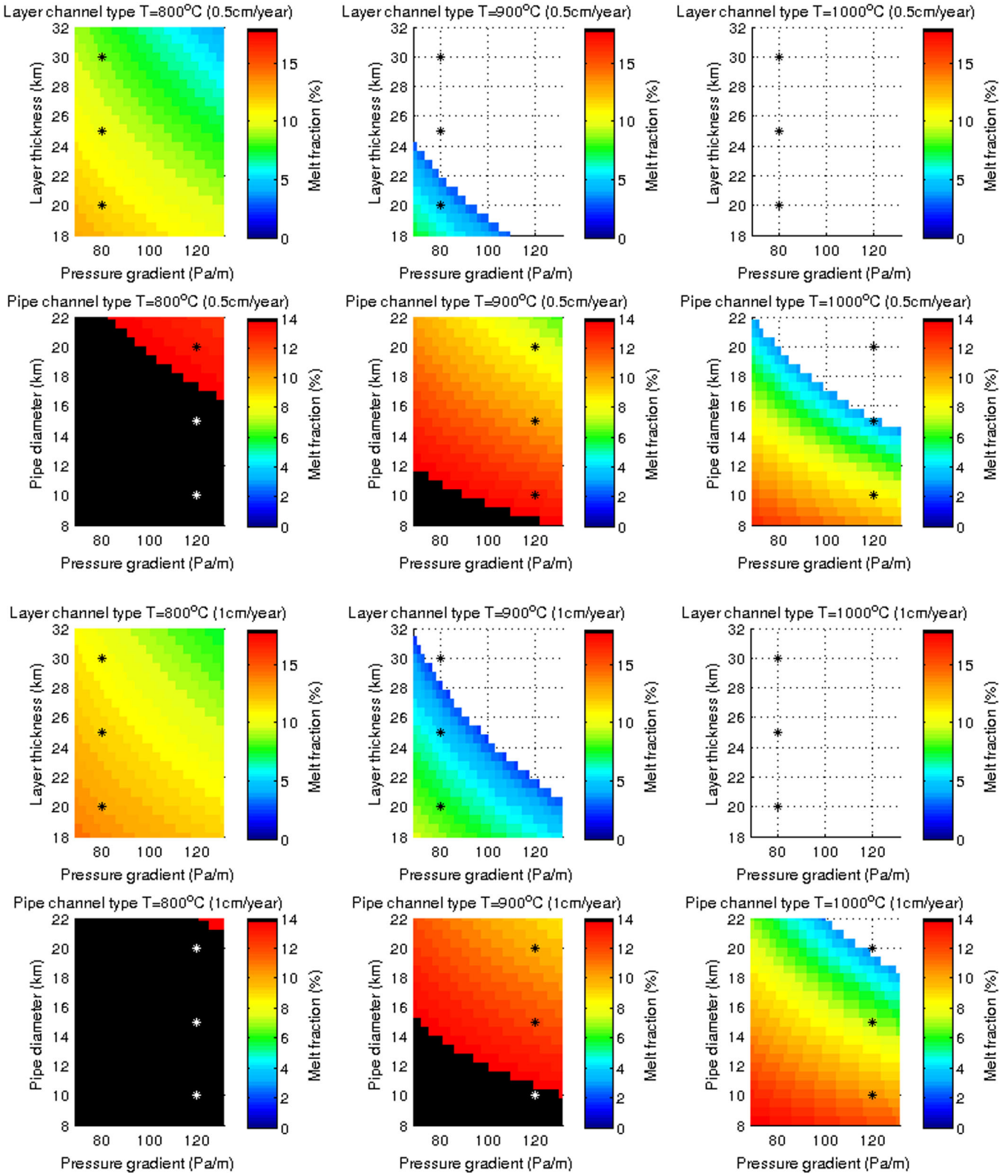

Figure 10. Minimum melt fractions associated with domination of Poiseuille flow based on method B. A reference pressure gradient of 80 Pa/s is associated with the Sonpgan-Ganzi area (layer model). A reference pressure gradient of 120 Pa/m is defined for the Kunlun area (pipe model) due to the steep decrease in topography further north. The black areas represent the melt fractions above the upper limit determined for the melt fraction in the Songpan-Ganzi (18%) and Kunlun (14%) areas. The white area represents conditions for which the Poiseuille velocity is above the Couette threshold even without presence of partial melt.

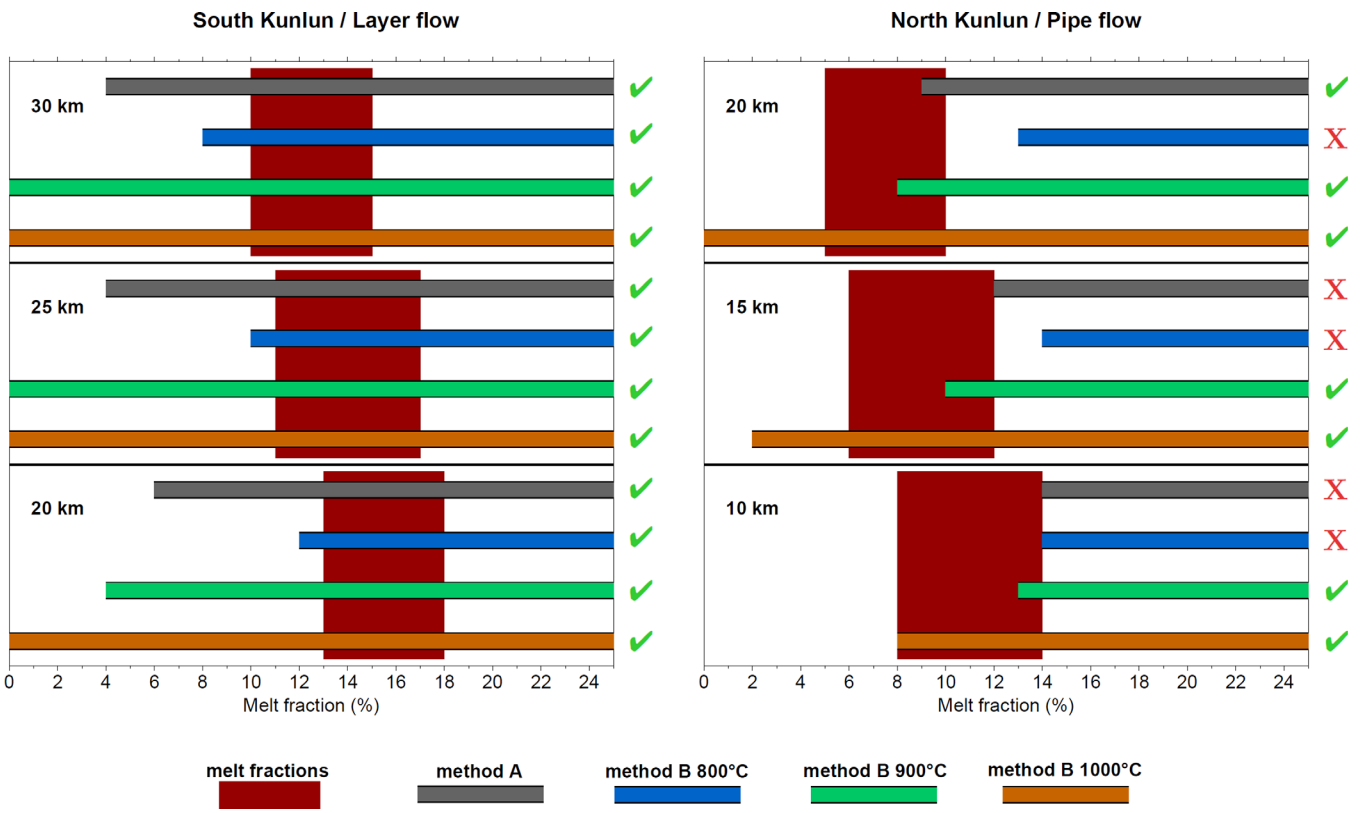

Figure 11. Validity check on Poiseuille flow driven by pressure gradient for both Songpan-Ganzi (South of the Kunlun Fault) and Kunlun (North of the Kunlun Fault) areas as a function of layer/pipe thickness/diameter. Melt fractions derived from resistivity and viscosity are compared with the melt fraction thresholds defined by method A and method B.

characteristic of the Songpan-Ganzi needs to be extrapolated into a surface flux from equation (6) by multiplying the latter with the width w of the layer (Figure 6). The proportion of flux oriented to the north can then be directly derived from the ratio of surface flux in both Songpan-Ganzi and Kunlun area, and is expressed as:

$$F = \frac{Q_{north}}{Q} = \frac{kQ_{pipe}}{wQ_{layer}}, \tag{12}$$

where w represents the width of the layer flow and k defines the number of pipes likely to be distributed over the width w. We assume a channel layer thickness of 20 km associated with a pressure gradient of 80 Pa/s in the Songpan-Ganzi crust and a channel pipe diameter of 20 km associated with a pressure gradient of 120 Pa/s in the Kunlun crust. The proportion of crustal flow directed north is determined as a function of the number of pipes over a width w of 100 km and a maximum number of three pipes. As seen in Table 2, defining a particular value of temperature or melt fraction characteristic of each area remains difficult. Consequently, discussing relative variations of those two parameters between the two areas of interest is preferred instead of using absolute values (Figure 12). However, as a reference, the melt fractions and temperature chosen for the calculations are, respectively, 10% and 900°C. The value of 10% was chosen since it represents a lower limit for the main flux Q in the Songpan-Ganzi terrane, whereas 10% is close to the upper limit for the Kunlun block, the flow proportion considered can be related to an upper estimation. The temperature of 900°C was chosen as a reference since it is likely common to both areas, but it also appears as the lower limit for channel flow to occur north of the Kunlun fault system. The effects of the deviations from those two values are presented in Figure 12.

The observations may not be reflecting the exact reality and more studies on the problem are definitely needed to obtain better constraints, but the results highlighted through this study are informative. With no variations in melt fractions and temperature between the Songpan-Ganzi and Kunlun crust, the two methods A and B can be compared, and they show similar maximum proportions with 15% for method A and

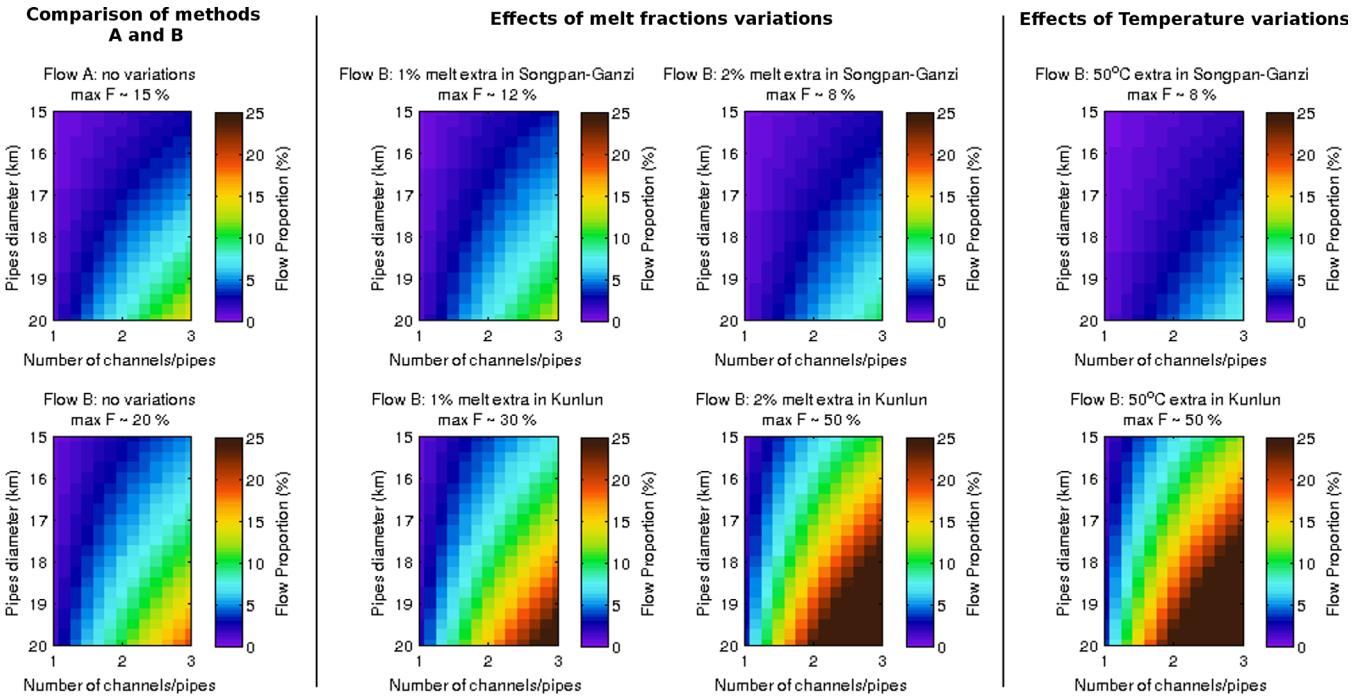

Figure 12. Estimations of the proportion of crustal flow injected north of the Kunlun fault as a function of pipe diameter and pipe numbers.

20% for method B. In method A, for both flux Q and Q_{north} a median value based on each of the laboratory studies was determined and then used for the estimations of F. Due to the form of equation (9), it is important to note that for method B, having no variations in melt and temperature between the two areas means the ratio F will be independent of either parameters. Therefore, the variations of melt and temperature between Songpan-Ganzi and Kunlun are independent of the reference chosen for method B. For this reason, the effects of melt and temperature will only be discussed for method B (Figure 12).

There are some observations that can be made about the effect of melt fractions. First of all, an increase in melt fraction in the Kunlun area compared to a similar increase in the Songpan-Ganzi will have far more impact on the resulting flow proportion migrating north. Furthermore, whereas an increase of melt of 2% in the Kunlun area raises the maximum proportion by 30%, it only decreases it by 12% for a similar increase in the Songpan-Ganzi area. Finally, the effect of the exponential part function of melt fraction of equation (9) can be clearly seen in the ratio Q_{north}/Q, since a variation of 1%–2% in opposition to a variation of 0%–1% will be more significant for the Kunlun area. For similar variations, an opposite effect is seen in the Songpan-Ganzi (Figure 12). The temperature variations between the two areas are quite comparable to the effects associated with melt. This is mainly due to the fact that temperature is also associated with an exponential component in the flow law used in method B (equation (9)). For instance, an increase in temperature beneath the Kunlun will also have quite a substantial impact on the quantity F compared to an increase of temperature in the Songpan-Ganzi area. It is also interesting to notice that a variation of 50°C between the north and south areas will have almost the same effect on F as a variation of around 2% in melt fraction.

Finally, the number of pipes, as well as their diameter, appears to be even more important than the melt fraction and temperature. For example, in the case of an increase of 1% in the melt fraction beneath the north Kunlun area, for a three pipes configuration a diameter reduction of 20–15 km reduces the flow proportions from 30% to 8%. Similarly, for the same example with a pipe diameter of 20 km, a reduction of pipe numbers from three to one reduces the flow proportion from 30% to almost 3%. It is less likely that the fraction of melt is higher in the Kunlun area, although processes such a strain heating [*Nabelek et al.*, 2010] could increase temperature and induce higher melting. As seen in Figure 12, with a temperature differential of 50°C higher the flow through three pipes of 20 km almost doubles compared to the flow for a constant temperature between south and north. In the 3-D modeling of MT data presented in *Wei et al.* [2014], we highlighted that over a width of some 100 km there could be two channels of at least 20 km diameter. If no variations in the

melt fractions and temperature between the south and north are assumed along the channels, according to Figure 12 the proportion of crustal flow migrating north could be of at least 10%. This is not significant but it could characterize the premise of the extension of the plateau further north.

7. Conclusions

We have outlined constraints on the crustal flow beneath Northern Tibet based on estimates of partial melt obtained from electrical conductivity and viscosity models. Our estimates of the partial melt in the Songpan-Ganzi area and the Kunlun area are 10–18% and 5–14% respectively. The consistencies between two different approaches for deriving flow velocities reveal interesting features that are believed to be robust.

For the Songpan-Ganzi area, the analyses have shown that for the corresponding melt fractions and temperatures, there are no restrictions at all on topography-driven channel flow to be dominant in the crust and, as the temperatures get closer to 1000°C, partial melt is not even needed to favor flow.

In the transition zone defined by the Kunlun area, channel injection driven by pressure gradients is more than likely occurring beneath the southern Kunlun ranges for temperatures of around 900°C.

Whereas beneath the Kunlun fault such temperatures are definitely present to facilitate crustal injection across the fault, the crust of the north Kunlun ranges at the vicinity of the boundary of the Qaidam basin, and associated with colder conditions, may represent only an early stage in the process. Channel injection beneath the Kunlun fault is likely triggering dehydration melting leading to thickening of the channel and favoring migration of the crustal flow further north. So far, by assuming no variations in melt content and temperature between the Songpan-Ganzi crust and the crust of the south Kunlun ranges, in northern Tibet at least 10% of crustal flow could be injected in the transition zone characterizing the northern margin of the plateau.

A number of different parameters were considered in this study, some of which are poorly defined. Therefore uncertainties still remain on the evolution of crustal flow beneath northern Tibet. However, the overarching conclusions we have reached are unlikely to be modified in any serious manner through more exhaustive and comprehensive examination.

Acknowledgments
We would like to acknowledge research funding from Science Foundation of Ireland (SFI, award 08/RFP/GEO1693 to A.G.J.), the NSF Continental Dynamics program and an NSERC Discovery Grant to Martyn Unsworth. We thank Larry Brown (Cornell University) for his leadership of INDEPTH-IV. We thank the Editor of G-cubed for his timely handling of our paper, and especially the two reviewers for their very supportive, insightful and useful comments that improved this paper. All data for this paper is properly cited and referred to in the reference list.

References

Ader et al. (2012), Convergence rate across the Nepal Himalaya and interseismic coupling on the Main Himalayan Thrust: Implications for seismic hazard, *J. Geophys. Res.*, *117*, B04403, doi:10.1029/2011JB009071.
Agius, M. R., and S. Lebedev (2013), Tibetan and Indian lithospheres in the upper mantle beneath Tibet: Evidence from broadband surface-wave dispersion, *Geochem. Geophys. Geosyst.*, *14*, 4260–4281, doi:10.1002/ggge.20274.
Agius, M. R., and S. Lebedev (2014), Shear velocity structure, radial anisotropy and dynamics of the Tibetan crust, *Geophys. J. Int.*, *199*, 1395–1415.
Annen, C., and R. S. J. Sparks (2002), Effects of repetitive emplacement of basaltic intrusions on thermal evolution and melt generation in the crust, *Earth Planet. Sci. Lett.*, *203*, 937–955.
Arzi, A. (1978), Critical phenomenon in the rheology of partially melted rocks, *Tectonophysics*, *44*, 173–184.
Bai, D., et al. (2010), Crustal deformation of the eastern Tibetan plateau revealed by magnetotelluric imaging, *Nat. Geosci.*, *3*, 358–362.
Beaumont, C., R. A. Jamieson, M. H. Nguyen, and B. Lee (2001), Himalayan tectonics explained by extrusion of a low-viscosity channel coupled to focused surface denudation, *Nature*, *414*, 738–742.
Bird, P. (1991), Lateral extrusion of lower crust from under high topography, in the isostatic limit, *J. Geophys. Res.*, *96*, 10,275–10,286.
Caldwell, W. B., S. L. Klemperer, S. S. Rai, and J. F. Lawrence (2009), Partial melt in the upper-middle crust of the northwest Himalaya revealed by Rayleigh wave dispersion, *Tectonophysics*, *477*(1–2), 58–65.
Christensen, N. I., and W. D. Mooney (1995), Seismic velocity structure and composition of the continental crust: A global view, *J. Geophys. Res.*, *100*, 9761–9788.
Clark, M. K., and L. H. Royden (2000), Topographic ooze: Building the eastern margin of Tibet by lower crustal flow, *Geology*, *28*, 703–706.
Clemens, J. D., and D. Vielzeuf (1987), Constraints on melting and magma production in the crust, *Earth Planet. Sci. Lett.*, *86*, 287–306.
Comeau, M. J., M. J. Unsworth, F. Ticona, and M. Sunagua (2015), Magnetotelluric images of magma distribution beneath Volcán Uturuncu, Bolivia: Implications for magma dynamics, *Geology*, *43*, 243–246.
Costa, A., L. Caricchi, and N. Bagdassarov (2009), A model for the rheology of particle-bearing suspensions and partially molten rocks, *Geochem. Geophys. Geosyst.*, *10*, Q03010, doi:10.1029/2008GC002138.
Gaillard, F. (2004), Laboratory measurements of electrical conductivity of hydrous and dry silicic melts under pressure, *Earth Planet. Sci. Lett.*, *218*(1–2), 215–228.
Gaillard, F., and G. I. Marziano (2005), Electrical conductivity of magma in the course of crystallization controlled by their residual liquid composition, *J. Geophys. Res.*, *110*, B06204, doi:10.1029/2004JB003282.
Gaillard, F., B. Scaillet, and M. Pichavant (2004), Evidence for present-day leucogranite pluton growth in Tibet, *Geology*, *32*, 801–804.
Gan, W., P. Zhang, Z. K. Shen, Z. Niu, M. Wang, Y. Wan, D. Zhou, and J. Cheng (2007), Present-day crustal motion within the Tibetan Plateau inferred from GPS measurements, *J. Geophys. Res.*, *112*, B08416, doi:10.1029/2005JB004120.

Gao, R., H. Wang, A. Yin, S. Dong, Z. Kuang, A. V. Zuza, W. Li, and X. Xiong (2013), Tectonic development of the northeastern Tibetan Plateau as constrained by high-resolution deep seismic reflection data, *Lithosphere*, *5*, 555–574.
Goldfarb, R. J., L. W. Snee, L. D. Miller, and R. J. Newberry, (1991), Rapid dewatering of the crust deduced from ages of mesothermal gold deposits, *Nature*, *354*, 296–298.
Grujic, D. (2006), Channel flow and continental collision tectonics: An overview, in *Channel Flow, Ductile Extrusion and Exhumation in Continental Collision Zones*, edited by R. D. Law, M. P. Searle, and L. Godin, *Geol. Soc., Spec. Publ.*, 268, 147–164.
Guo, Z., M. Wilson, J. Liu, and Q. Mao (2006), Post-collisional, potassic and ultrapotassic magmatism of the northern Tibetan plateau: Constraints on characteristics of the mantle source, geodynamic setting and uplift mechanisms, *J. Petrol.*, *47*, 1177–1220.
Hacker, B. R., E. Gnos, L. Ratschbacher, M. Grove, M. McWilliams, S. V. Sobolev, J. Wan, and W. Zhenhan (2000), Hot and dry deep crustal xenoliths from Tibet, *Science*, *287*, 2463–2466.
Hacker, B. R., M. H. Ritzwoller, and J. Xie (2014), Partially melted, micabearing crust in Central Tibet, *Tectonics*, *33*, 1408–1424, doi:10.1002/2014TC003545.
Haines, S. S., S. L. Klemperer, L. Brown, G. Jingru, J. Mechie, R. Meissner, A. Ross, and Z. Wenjin (2003), INDEPTH III seismic data: From surface observations to deep crustal processes in Tibet, *Tectonics*, *22*(1), 1001, doi:10.1029/2001TC001305.
Harrison, T. M. (2006). Did the Himalayan Crystallines extrude partially molten from beneath the Tibetan Plateau?, in *Channel Flow, Ductile Extrusion and Exhumation in Continental Collision Zones*, edited R. D. Law, M. P. Searle, and L. Godin *Geol. Soc. Spec. Publ.*, 268, 237–254.
Hashin, Z., and A. Shtrikman (1962), A variational approach to the theory of effective magnetic permeability of multiphase materials, *J. Appl. Phys.*, *33*, 3125–3131.
Hess, K. U., and D. B. Dingwell (1996), Viscosities of hydrous leucogranite melts: A non-Arrhenian model, *Am. Mineral.*, *81*, 1297–1300.
Holtz, F., W. Johannes, N. Tamic, and H. Behrens (2001), Maximum and minimum water contents of granitic melts generated in the crust: A reevaluation and implications, *Lithos*, *56*, 1–14.
Jamieson, R. A., M. J. Unsworth, N. B. W. Harris, C. L. Rosenberg, and K. Schulmann (2011), Crustal melting and the flow of mountains, *Elements*, *7*, 253–260.
Jiang, C., Y. Yang, and Y. Zheng (2014), Penetration of mid-crustal low velocity zone across the Kunlun Fault in the NE Tibetan Plateau revealed by ambient noise tomography, *Earth Planet. Sci. Lett.*, *406*, 81–92.
Jimenez-Munt, I., M. Fernandez, J. Verges, and J. P. Platt (2008), Lithosphere structure underneath the Tibetan Plateau inferred from elevation, gravity and geoid anomalies, *Earth Planet. Sci. Lett.*, *267*, 276–289.
Jones, A. G. (1992), Electrical conductivity of the continental lower crust, in *The Continental Lower Crust*, edited by D. M. Fountain, R. J. Arculus, and R. W. Kay, pp. 81–143, Elsevier, N. Y.
Kariya, K. A., and T. J. Shankland, (1983), Electrical conductivity of dry lower crustal rocks, *Geophysics*, *48*, 52–61.
Karplus, M. S., W. Zhao, S. L. Klemperer, Z. Wu, J. Mechie, D. Shi, L. D. Brown, and C. Chen (2011), Injection of Tibetan crust beneath the south Qaidam Basin: Evidence from INDEPTH IV wide-angle seismic data, *J. Geophys. Res.*, *116*, B07301, doi:10.1029/2010JB007911.
Klemperer, S. (2006), Crustal flow in Tibet: Geophysical evidence for the physical state of Tibetan lithosphere, and inferred patterns of active flow, in *Channel Flow, Ductile Extrusion and Exhumation in Continental Collision Zones* edited by R. D. Law, M. P. Searle, and L. Godin, *Geol. Soc. Spec. Publ.*, 268, 39–70.
Le Pape, F., A. G. Jones, J. Vozar, and W. Wenbo (2012), Penetration of crustal melt beyond the Kunlun Fault into northern Tibet, *Nat. Geosci.*, *5*, 330–335.
Li, S., M. J. Unsworth, J. R. Booker, W. Wei, H. Tan, and A. G. Jones (2003), Partial melt or aqueous fluids in the Tibetan crust: Constraints from INDEPTH magnetotelluric data, *Geophys. J. Int.*, *153*, 289–304.
Mackie, R. L. (2002), User manual and software documentation for two-dimensional inversion of magnetotelluric data, in *Anisotropy Version 6.7*, GSY-USA Inc., San Francisco, Calif.
Makovsky, Y., and S. Klemperer (1999), Measuring the seismic properties of Tibetan bright spots: Evidence for free aqueous fluids in the Tibetan middle crust, *J. Geophys. Res.*, *104*, 10,795–10,825.
Mandolesi, E., M. Moorkamp, and A. G. Jones (2014), A study on the influence of conductive paths and their direction in randomly generated conductor network, American Geophysical Union, Abstract MR23B-4359 presented at 2014 Fall Meeting, AGU, San Francisco, Calif.
McKenna, L. W., and J. D. Walker (1990), Geochemistry of crustally derived leucogranitic igneous rocks from the Ulugh Muztagh area, Northern Tibet and their implications for the formation of the Tibetan Plateau, *J. Geophys. Res.*, *95*, 21,483–21,502.
Mechie, J., S. V. Sobolev, L. Ratschbacher, A. Y. Babeyko, G. Bock, A. G. Jones, K. D. Nelson, K. D. Solon, L. D. Brown, and W. Zhao (2004), Precise temperature estimation in the tibetan crust from seismic detection of the α-β quartz transition, *Geology*, *32*, 601–604.
Mecklenburgh, J., and E. H. Rutter (2003), On the rheology of partially molten synthetic granite, *J. Struct. Geol.*, *25*, 1575–1585.
Medvedev, S., and C. Beaumont (2006), Growth of continental plateaus by channel injection: Models designed to address constraints and thermomechanical consistency, in *Channel Flow, Ductile Extrusion and Exhumation in Continental Collision Zones* edited by R. D. Law, M. P. Searle, and L. Godin, *Geol. Soc. Spec. Publ.*, 268, 147–164.
Mueller, H. J., and H. J. Massonne (2001), Experimental high pressure investigation of partial melting in natural rocks and their influence on Vp and Vs, *Phys. Chem. Earth A*, *26*, 325–332.
Nabelek, J., G. Hetenyi, J.Vergne, S. Sapkota, B. Kafle, M. Jiang, H. Su, J. Chen, and B. S. Huang (2009), the Hi-CLIMB Team Underplating in the Himalaya-Tibet collision zone revealed by the Hi-CLIMB Experiment, *Science*, *325*, 1371–1374.
Nabelek, P. I., A. G. Whittington, and A. M. Hofmeister (2010), Strain heating as a mechanism for partial melting and ultrahigh temperature metamorphism in convergent orogens: Implications of temperature-dependent thermal diffusivity and rheology, *J. Geophys. Res.*, *115*, B12417, doi:10.1029/2010JB007727.
Nelson, K. D., et al. (1996), Partially molten middle crust beneath southern Tibet: Synthesis of project INDEPTH results, *Science*, *274*(5293), 1684–1688.
Owens, T. J., and G. Zandt (1997), Implications of crustal property variations for models of Tibetan plateau evolution, *Nature*, *387*, 37–43.
Partzsch, G. M., F. R. Schilling, and J. Arndt (2000), The influence of partial melting on the electrical behavior of crustal rocks: Laboratory examinations, model calculations and geological interpretations, *Tectonophysics*, *317*, 189–203.
Patiño Douce, A. E., and T. C. McCarthy (1998), Melting of crustal rocks during continental collision and subduction, in *When Continents Collide:Geodynamics and Geochemistry of Ultrahigh-Pressure Rocks*, chap. 2, edited by B. R. Hacker and J. G. Liou, pp. 27–55, Kluwer Acad., Netherlands.
Pommier, A., and E. L. Trong (2011), SIGMELTS: A web portal for electrical conductivity calculations in geosciences, *Comput. Geosci.*, *37*, 1450–1459.
Pommier, A. F., R. L. Evans, K. Key, J. A. Tyburczy, and S. M. J. Elsenbeck (2013), Prediction of silicate melt viscosity from electrical conductivity: A model and its geophysical implications, *Geochem. Geophys. Geosyst.*, *14*, 1685–1692, doi:10.1002/ggge.20103.

Rippe, D., and M. Unsworth (2010), Quantifying crustal flow in Tibet with magnetotelluric data, *Phys. Earth Planet. Inter.*, *179*, 107–121.
Roberts, J. J., and J. A. Tyburczy (1999), Partial-melt electrical conductivity: Influence of melt composition, *J. Geophys. Res.*, *104*, 7055–7065.
Rosenberg, C. L., and M. R. Handy (2005), Experimental deformation of partially melted granite revisited: Implications for the continental crust, *J. Metamorph. Geol.*, *23*, 19–28.
Royden, L. H., B. C. Burchfiel, R. W. King, E. Wang, Z. Chen, F. Shen, and Y. Liu (1997), Surface deformation and lower crustal flow in eastern Tibet, *Science*, *276*, 788–790.
Rushmer, T. (1995), An experimental deformation study of partially molten amphibolite: Application to low-melt fraction segregation, *J. Geophys. Res.*, *100*, 15,681–15,695.
Rutter, E. H., and D. H. K. Neumann (1995), Experimental deformation of partially molten Westerly granite under fluid-absent conditions, with implications for the extraction of granitic magmas, *J. Geophys. Res.*, *100*, 15,697–15,715.
Rutter, E. H., K. H. Brodie, and D. H. Irving (2006), Flow of synthetic, wet, partially molten "granite" under undrained conditions: An experimental study, *J. Geophys. Res.*, *111*, B06407, doi:10.1029/2005JB004257.
Rutter, E. H., J. Mecklenburgh, and K. H. Brodie (2011), Rock mechanics constraints on mid-crustal low-viscosity flow beneath Tibet, *Geol. Soc. Spec. Publ.*, *360*, 329–336.
Ryder, I., R. Burgmann, and F. Politz (2011), Lower crustal relaxation beneath the Tibetan Plateau and Qaidam Basin following the 2001 Kokoxili earthquake, *Geophys. J. Int.*, *187*, 613–630.
Schilling, F. R., and G. M. Partzsch (2001), Quantifying partial melt fraction in the crust beneath the central Andes and the Tibetan Plateau, *Phys. Chem. Earth A*, *26*, 239–246.
Schmeling, H. (1985), Numerical models on the influence of partial melt on elastic, anelastic and electric properties of rocks, Part I: Elasticity and anelasticity, *Phys. Earth Planet. Inter.*, *41*, 34–57.
Scott, T., and D. L. Kohlstedt (2006), The effect of large melt fraction on the deformation behavior of peridotite, *Earth Planet. Sci. Lett.*, *246*, 177–187.
Searle, M. P., J. R. Elliott, R. J. Phillips, and S. L. Chung (2011), Crustal-lithospheric structure and continental extrusion of Tibet, *J. Geol. Soc. London*, *168*, 633–672.
Takei, Y. (2000), Acoustic properties of partially molten media studied on a simple binary system with a controllable dihedral angle. *J. Geophys. Res.*, *105*, 16,665–16,682.
Taylor, M. A. J., and S. C. Singh (2002), Composition and microstructure of magma bodies from effective medium theory, *Geophys. J. Int.*, *149*, 15–21.
ten Grotenhuis, S. M., M. R. Drury, C. J. Spiers, and C. J. Peach (2005), Melt distribution in olivine rocks based on electrical conductivity measurements, *J. Geophys. Res.*, *110*, B12201, doi:10.1029/2004JB003462.
Tozer, D.C., (1979), The interpretation of upper-mantle electrical conductivities, *Tectonophysics*, *56*, 147–163.
Tozer, D.C., (1981), The mechanical and electrical properties of the Earth's asthenosphere, *Phys. Earth Planet. Int.*, *25*, 280–296.
Turcotte, D. L., and G. Schubert (2014), *Geodynamics*, 3rd ed., Cambridge Univ. Press, Cambridge, U. K.
Turner, S., N. Arnaud, J. Liu, N. Rogers, C. Hawkesworth, N. Harris, S. Kelley, P. van Calsteren, and W. Deng (1996), Postcollision, shoshonitic volcanism on the Tibetan plateau: Implications for convective thinning of the lithosphere and the source of ocean island basalts, *J. Petrol.*, *37*, 45–71.
Unsworth, M., A. G. Jones, W. Wei, G. Marquis, S. G. Gokarn, J. E. Spratt, and I.-M. Team (2005), Crustal rheology of the Himalaya and southern Tibet inferred from magnetotelluric data, *Nature*, *438*, 78–81, doi:10.1038/nature04154.
van der Molen, I., and M. Patterson (1979), Experimental deformation of partially melted granite, *Contrib. Mineral. Petrol.*, *70*, 299–318.
Vergne, J., G. Wittlinger, V. Farra, and H. Su (2002), Evidence for upper crustal anisotropy in the Songpan Ganze (northeastern Tibet) terrane, *Earth Planet. Sci.*, *203*, 25–33.
Vozar, J., A. G. Jones, J. Fullea, M. R. Agius, S. Lebedev, F. Le Pape, and W. Wei (2014), Integrated geophysical-petrological modeling of lithosphere-asthenosphere boundary in central Tibet using electromagnetic and seismic data, *Geochem. Geophys. Geosyst.*, *15*, 3965–3988, doi:10.1002/2014GC005365.
Wang, C., J. Dai, X. Zhao, Y. Li, S. A. Graham, D. He, B. Ran, and J. Meng (2014), Outward-growth of the Tibetan Plateau during the Cenozoic: A review, *Tectonophysics*, *621*, 1–43.
Wang, C. S., R. Gao, A. Yin, H. Y. Wang, Y. X. Zhang, T. Guo, Q. Li, and Y. L Li (2011), A mid-crustal strain-transfer model for continental deformation: A new perspective from high-resolution deep seismic-reflection profiling across NE Tibet, *Earth Planet. Sci. Lett.*, *306*, 279–288.
Wang, Q., F. McDermott, J. F. Xu, H. Bellon, and Y. Zhu (2005), Cenozoic k-rich adakitic volcanic rocks in the Hohxil area, northern Tibet: Lower-crustal melting in an intracontinental setting, *Geology*, *33*, 465–468.
Wang, Q., S. L. Chung, X. H. Li, D. Wyman, Z. X. Li, W. D. Sun, H. N. Qiu, Y. S. Liu, and Y. T. Zhu (2012), Crustal melting and flow beneath Northern Tibet: Evidence from Mid-Miocene to quaternary strongly Peraluminous Rhyolites in the Southern Kunlun Range, *J. Petrol.*, *53*, 2523–2566.
Watanabe, T., and K. Kurita (1993), The relationship between electrical conductivity and melt fraction in a partially molten system: Archie's law behaviour, *Phys. Earth Planet. Inter.*, *78*, 9–17.
Wei, W., S. Jin, G. Ye, M. Deng, H. Tan, M. Unsworth, J. Booker, A. G. Jones, and S. Li (2007), Features of faults in the central and northern Tibetan plateau based on results of INDEPTH (III)-MT, *Front. Earth Sci. China*, *1*(1), 121–128.
Wei, W., F. L. Pape, A. G. Jones, J. Vozar, H. Dong, M. J. Unsworth, S. Jin, G. Ye, J. Jing, L. Zhang, and C. Xie (2014), Northward channel flow in northern Tibet revealed from 3D magnetotelluric modeling, *Phys. Earth Planet. Inter.*, *235*, 13–24.
Whittington, A. G., A. M. Hofmeister, and P. I. Nabelek (2009), Temperature-dependent thermal diffusivity of the earth's crust and implications for magmatism, *Nature*, *458*, 319–321.
Yang, Y., M. H. Ritzwoller, Y. Zheng, W. Shen, A. L. Levshin, and Z. Xie (2012), A synoptic view of the distribution and connectivity of the mid-crustal low velocity zone beneath Tibet, *J. Geophys. Res.*, *117*, B04303, doi:10.1029/2011JB008810.
Yardley, B. W. D., (1991), Isotope dating: Quick shifts in plate motion, *Nature*, *354*, 269–270.
Yardley, B. W. D., and W. Valley (1997). The petrologic case for a dry lower crust. *J. Geophys. Res.*, *102*, 12,173–12,185.
Yoshino, T., and F. Noritake (2011), Unstable graphite films on grain boundaries in crustal rocks, *Earth Planet. Sci. Lett.*, *306*, 186–192.
Yu, L., R. L. Evans, and R. N. Edwards (1997), Transient electromagnetic responses in seafloor with triaxial anisotropy, *Geophys. J. Int.*, *129*, 292–304.